

## 14. SITE 1086<sup>1</sup>

### Shipboard Scientific Party<sup>2</sup>

#### HOLE 1086A

**Position:** 31°33.1608'S, 15°39.6235'E  
**Start hole:** 1900 hr, 1 October 1997  
**End hole:** 0925 hr, 2 October 1997  
**Time on hole:** 14.42 hr  
**Seafloor (drill pipe measurement from rig floor, mbrf):** 792.8  
**Total depth (drill pipe measurement from rig floor, mbrf):** 999.0  
**Distance between rig floor and sea level (m):** 11.7  
**Water depth (drill pipe measurement from sea level, m):** 781.1  
**Penetration (mbsf):** 206.2  
**Coring totals:**  
Type: APC  
Number: 22  
Cored: 206.2 m  
Recovered: 211.09 m (102.37%)  
**Lithology:**  
Unit I: clay-rich nannofossil-foraminifer ooze, foraminifer-nannofossil ooze, foraminifer-rich nannofossil ooze, and nannofossil ooze

#### HOLE 1086B

**Position:** 31°33.1588'S, 15°39.6047'E  
**Start hole:** 0925 hr, 1 October 1997  
**End hole:** 0030 hr, 3 October 1997  
**Time on hole:** 15.08 hr  
**Seafloor (drill pipe measurement from rig floor, mbrf):** 796.2  
**Total depth (drill pipe measurement from rig floor, mbrf):** 1004.7  
**Distance between rig floor and sea level (m):** 11.7  
**Water depth (drill pipe measurement from sea level, m):** 784.5  
**Penetration (mbsf):** 208.5  
**Coring totals:**  
Type: APC  
Number: 23  
Cored: 208.5 m  
Recovered: 212.09 m (101.72%)  
**Lithology:**  
Unit I: clay-rich nannofossil-foraminifer ooze, foraminifer-nannofossil ooze, foraminifer-rich nannofossil ooze, and nannofossil ooze  
**Principal results:** Site 1086 is located in the southernmost area of the Cape Basin in ~780 m deep water. The primary objective for drilling at this site

is to explore the early history of the Benguela Current in the Southern Cape Basin (SCB) and to detect possible Agulhas Current influences. We expect to obtain information about the supply of warm water from the Indian Ocean, through the Agulhas Retroflexion, and from the Subtropical Convergence Zone, which are nearby. Both warm-water and cold-water eddies can be shed from the retroflexion and the front, but the position of the Subtropical Convergence Zone and the transport by the Benguela Current will be crucial in determining which type of eddy is more likely to reach the site. The site also is located close to the continent and should detect upwelling signals and signals from continental climates, as well as sea-level changes.

Two holes were cored with the advanced hydraulic piston corer (APC) at Site 1086 to a maximum depth of 212 meters below seafloor (mbsf), which recovered a relatively continuous hemipelagic sedimentary section spanning the lower Pleistocene to upper Miocene. Hole 1086A was cored with the APC to 206 mbsf. Hole 1086B was cored with the APC to 212 mbsf.

The upper Pleistocene record apparently is missing. Sediments form one lithostratigraphic unit and are composed of clay-rich nannofossil-foraminifer ooze, foraminifer-nannofossil ooze, foraminifer-rich nannofossil ooze, and nannofossil ooze. Most of the sediment is moderately bioturbated, and burrows range in diameter from 1 mm to more than 1 cm. The detrital component is dominated by clay and trace abundances of silt-sized, subangular mono- and polycrystalline quartz grains. Authigenic minerals are rare or present in trace abundances. Pyrite is present as silt-sized aggregates of euhedral crystals or as framboids. The biogenic component in all smear slides consists of abundant to very abundant nannofossils. Foraminifers are abundant to common.

Sedimentation rates are ~35 m/m.y. between 120 and 200 mbsf (Miocene to lower Pliocene) and are much lower (20 m/m.y.) in the upper Pliocene and Pleistocene intervals.

Calcareous nannofossils and planktonic foraminiferal datums are in good agreement. Siliceous microfossils are rare or absent in much of the sediment. A significant amount of tropical to subtropical planktonic foraminiferal species between 140 and 150 mbsf may indicate a warming event or increased input from the warm Agulhas Current. There are only a few radiolarian species at 25 mbsf; this suggests a warm and low-productivity ocean. Dinoflagellate cysts are common in the upper Miocene sediment between 140 and 206 mbsf (~5.9–7.5 Ma).

Except for the uppermost 30 mbsf the cores show significant coring-induced remagnetization. The magnetostratigraphic interpretation at Site 1086 is based mainly on the inclinations after alternating-field (AF) demagnetization at 20 mT. All chrons from the Olduvai (C2n) to C4n (~7.5 Ma) were identified.

Detailed comparisons between the magnetic susceptibility records generated on the multisensor track (MST) and color reflectance measured with the Minolta spectrophotometer demonstrated complete recovery of the sedimentary sequence down to 232 meters composite depth (mcd).

Sediments from Site 1086 are low in marine organic matter, with total organic carbon (TOC) concentrations fluctuating between 3.6 wt% and nil. Concentrations of calcium carbonate are generally between 85 and 75 wt%. The interstitial water composition is controlled dominantly by the high carbonate content and low organic carbon concentrations in the sediments. The chemical gradients at Site 1086 are even more gradual than those found at the lithologically similar Site 1085. For example, sulfate is

<sup>1</sup>Wefer, G., Berger, W.H., Richter, C., et al., 1998. *Proc. ODP, Init. Repts.*, 175: College Station, TX (Ocean Drilling Program).

<sup>2</sup>Shipboard Scientific Party is given in the list preceding the Table of Contents.

not completely consumed until 180 mbsf, which is the greatest depth observed so far during Leg 175, and the alkalinity maximum at 125 mbsf is only 17 mM. Carbonate and phosphate precipitation reactions are inferred from the profiles of dissolved calcium, magnesium, and phosphate.

Physical sediment properties were determined both by high-resolution MST core logging and index properties measurements. Magnetic susceptibility and gamma-ray attenuation porosity evaluator (GRAPE) signals reveal pronounced cyclicities.

Although the upper Quaternary record is missing, a continuous record back into the upper Miocene was recovered. Sedimentation rates are high in the lower part of the section, into the lower Pliocene sequence. Subsequently, rates drop until they reach zero in the lowermost Quaternary sediment. At the water depth near 800 m, the site records properties of (and activity within) the upper water layers in the Southern Cape Basin. Increased winnowing since the lower Pliocene is apparently reflected in the drop in sedimentation rate and results in an increasing proportion of sand fraction in the younger sediments.

## BACKGROUND AND OBJECTIVES

Sites 1086 and 1087 are located in the southernmost area of the Cape Basin. South of the proposed transect, the margin becomes too steeply sloped to support undisturbed sediments. The sedimentary records will help in exploring the early history of the Benguela Current in the SCB and in detecting possible Agulhas Current influences (Wefer et al., 1996). The warm-water inflow from the Indian Ocean is thought to be an important component of the global thermohaline circulation system (Gordon, 1986). It has been suggested that much of the North Atlantic Deep Water (NADW) leaving the Atlantic Ocean is balanced by a warm upper layer return flow from the Indian Ocean around the southern tip of Africa, and that this warm-water source turns on and off in tune with the glacial/interglacial fluctuations of NADW production (Berger et al., 1987; McIntyre et al., 1989). A competing model to the "warm-water route," the so-called "cold-water route" (Rintoul, 1991), postulates an inflow from the Pacific Ocean through the Drake Passage.

The sites in the SCB (Sites 1086 and 1087) are expected to deliver information about the supply of warm water from the Indian Ocean, through the Agulhas Retroflection, and from the Subtropical Convergence Zone, which are nearby (Fig. 1). Both warm-water and cold-water eddies can be shed from the retroflection and the front (Fig. 1), but the position of the Subtropical Convergence Zone and the transport by the Benguela Current will be crucial in determining which type of eddy is more likely to reach the sites. These incursions of warm- and cold-water masses will be documented by planktonic indicators (especially by diatoms and foraminifers, but also by nanofossils and radiolarians). One example that is documented for the late

Quaternary is the recolonization of the planktonic foraminifer *Globorotalia menardii* in the Atlantic after regional extinction during glacials (Berger et al., 1985).

Also, the sites are located close to the continent and should detect upwelling signals and signals from continental climates (pollen, clay minerals, and coarser terrigenous matter), as well as sea-level changes.

## OPERATIONS

### Hole 1086A (Proposed Site SCB-E)

The 157-nmi voyage to Site 1086 was accomplished at an average speed of 8.8 kt. The speed of the vessel was adversely affected because of the northward flowing Benguela Current and rough seas. The vessel approached the Global Positioning System coordinates of the site, and a beacon was deployed at 1900 hr on 1 October. Hole 1086A was spudded with the APC at 2240 hr. The seafloor depth was estimated from the recovery of the first core at 781.1 meters below sea level (mbsl). APC coring advanced without incident to 206.2 mbsf (Cores 175-1086-1H through 22H), which was considered refusal depth for piston coring. The recovery for the APC at Hole 1086A was 102.4% (Table 1; also see expanded coring summary table on CD-ROM, back pocket, this volume). Cores were oriented starting with Core 3H. Adara heat-flow measurements were not obtained at this site. The drill string was pulled out of the hole with the bit clearing the seafloor at 0925 hr on 2 October, thereby ending Hole 1086A.

### Hole 1086B

The vessel was offset 30 m to the west, and Hole 1086B was spudded with the APC at 1010 hr on 2 October. The recovery of the first core established the seafloor depth at 786.5 mbsl. APC cores 175-1086B-1H through 23H were taken from 0 to 212.1 mbsf, with 101.7% recovery (Table 1). The last core did not achieve a full piston stroke. Cores were oriented starting with Core 4H. The drill string was then retrieved, and with bit cleared the seafloor at 2230 hr. The beacon was recovered, the hydrophones and thrusters were retracted, and the vessel was under way to the next site at 0030 hr on 3 October.

## SITE GEOPHYSICS

### Introduction and Strategy

The decrease of terrigenous accumulation rates throughout the Tertiary was related to the aridification of the southern part of the African continent, which led to starved conditions in the Neogene for

Figure 1. Main mesoscale and larger features of circulation in the upper ocean layers of the region connecting the Indian and Atlantic Oceans. A = an Agulhas ring, recently shed from the Agulhas Retroflection (E), being encircled by an Agulhas filament; B = Agulhas rings drifting off into the South Atlantic; C = a cyclonic eddy forming part of a well-developed Natal Pulse on the Agulhas Current, causing an upstream retroflection (D) at the Agulhas Plateau. Solid circles = Leg 175 drill sites; open arrows = the large-scale, general background circulation of the subtropical gyres. From Lutjeharms (1996).

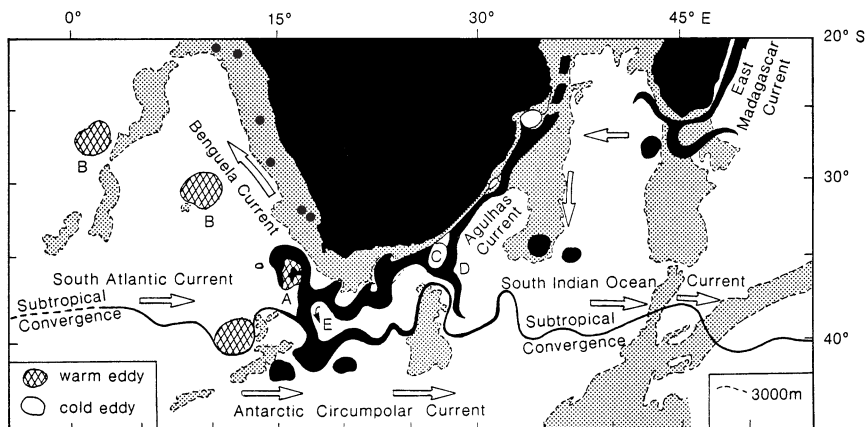


Table 1. Coring summary for Site 1086.

Core	Date (Oct 1997)	Time (UTC)	Interval (mbsf)	Length cored (m)	Length recovered (m)	Recovery (%)
175-1086A-						
1H	1	2245	0.0-6.7	6.7	6.77	101.0
2H	1	2320	6.7-16.2	9.5	7.97	83.9
3H	1	2350	16.2-25.7	9.5	10.00	105.3
4H	2	0015	25.7-35.2	9.5	10.00	105.3
5H	2	0035	35.2-44.7	9.5	7.95	83.7
6H	2	0100	44.7-54.2	9.5	10.02	105.5
7H	2	0120	54.2-63.7	9.5	10.01	105.4
8H	2	0145	63.7-73.2	9.5	9.94	104.6
9H	2	0210	73.2-82.7	9.5	9.90	104.2
10H	2	0235	82.7-92.2	9.5	10.01	105.4
11H	2	0300	92.2-101.7	9.5	9.90	104.2
12H	2	0325	101.7-111.2	9.5	9.89	104.1
13H	2	0345	111.2-120.7	9.5	9.71	102.2
14H	2	0410	120.7-130.2	9.5	9.33	98.2
15H	2	0435	130.2-139.7	9.5	9.89	104.1
16H	2	0515	139.7-149.2	9.5	10.08	106.1
17H	2	0545	149.2-158.7	9.5	9.95	104.7
18H	2	0615	158.7-168.2	9.5	9.94	104.6
19H	2	0640	168.2-177.7	9.5	10.01	105.4
20H	2	0700	177.7-187.2	9.5	10.02	105.5
21H	2	0745	187.2-196.7	9.5	9.89	104.1
22H	2	0815	196.7-206.2	9.5	9.91	104.3
Coring totals:				206.2	211.09	102.4
175-1086B-						
1H	2	1020	0-0.3	0.3	0.29	96.7
2H	2	1045	0.3-9.8	9.5	9.28	97.7
3H	2	1105	9.8-19.3	9.5	9.50	100.0
4H	2	1130	19.3-28.8	9.5	9.91	104.3
5H	2	1155	28.8-38.3	9.5	9.79	103.1
6H	2	1220	38.3-47.8	9.5	9.96	104.8
7H	2	1245	47.8-57.3	9.5	9.80	103.2
8H	2	1310	57.3-66.8	9.5	9.96	104.8
9H	2	1335	66.8-76.3	9.5	8.41	88.5
10H	2	1415	76.3-85.8	9.5	9.83	103.5
11H	2	1440	85.8-95.3	9.5	9.94	104.6
12H	2	1500	95.3-104.8	9.5	9.90	104.2
13H	2	1530	104.8-114.3	9.5	9.95	104.7
14H	2	1620	114.3-123.8	9.5	10.07	106.0
15H	2	1645	123.8-133.3	9.5	9.27	97.6
16H	2	1715	133.3-142.8	9.5	9.81	103.3
17H	2	1740	142.8-152.3	9.5	9.80	103.2
18H	2	1810	152.3-161.8	9.5	9.33	98.2
19H	2	1835	161.8-171.3	9.5	9.45	99.5
20H	2	1905	171.3-180.8	9.5	10.04	105.7
21H	2	1935	180.8-190.3	9.5	9.73	102.4
22H	2	2005	190.3-199.8	9.5	9.34	98.3
23H	2	2040	199.8-208.5	8.7	8.73	100.3
Coring totals:				208.5	212.09	101.7

Notes: UTC = Universal Time Coordinated. An expanded version of this coring summary table that includes lengths and depths of sections and comments on sampling is included on CD-ROM (back pocket, this volume).

the deeper part of the Cape Basin and the deposition of pelagic sediments at the continental margin. Neogene sedimentation was accompanied by successive slope failures (e.g., Dingle, 1980; Dingle and Robson, 1992) because of the buoyant behavior of the sediment-loaded margin. During the Pleistocene, a significant portion of the continental slope and rise was affected by further massive slumps, slides, and debris flows, and in many places the Neogene sedimentary column was partially or completely removed. This was observed at the two Deep Sea Drilling Project (DSDP) Sites 360 and 361 off Cape Town, and also in the working area of the Southern Cape Basin (SCB), as identified in the original seismic data of Austin and Uchupi (1982).

However, the SCB area remained a viable target for drilling because it is located at the southern rim of the Orange Fan. The underlying morphology created by the Orange River until the late Oligocene or Miocene modified the shape of the continental margin toward moderate slope angles. The working area in the SCB was chosen to study the onset and the early history of the Benguela Current and to detect possible influences of the Agulhas Current. The proximity to the continent allows the identification of local upwelling signals, sea-level changes, and a study of continental climate.

In the original proposal, three sites were selected from the seismic Line AM-54 by Austin and Uchupi (1982) for a depth transect. After the *Meteor* M34/1 seismic survey (Bleil et al., 1996), one high-priority site was chosen for APC and extended core barrel (XCB) coring down to 600 m sub-bottom depth, with additional alternate sites at different water depths (Fig. 2).

Two major reflectors can be used for a first chronostratigraphic assignment of seismic units. Seismic Reflector AII was first described by Emery et al. (1975) and later named Reflector P by Gerrard and Smith (1982). It was assigned a late Aptian age by Bolli et al. (1978), and it indicates the "earliest recognizable shelf-slope-rise relationship" (Dingle and Robson, 1992) in the Cape Basin. The second basinwide observable Reflector D (Emery et al., 1975; Reflector L of Gerrard and Smith, 1982) denotes a condensed section and a sharp downhole decrease in the contents of calcium carbonate at the Paleocene/Eocene boundary, according to drilling results of DSDP Leg 40 (Bolli et al., 1978).

## Seismostratigraphy

Altogether, eight seismic lines with a total length of 854 km were measured during *Meteor* Cruise M34/1 near the proposed site SCB-1 (Bleil et al., 1996). Bathymetric measurements revealed a significant variability in the morphology, which confirmed the existence of major slump events. A ridge-type structure is observed between the two Lines Geosciences Bremen (GeoB)/AWI 96-001 and 96-003. Slump scarps are identified (e.g., on Line GeoB/AWI 96-001 between 2000 and 2500 m water depth).

Major slump structures are known from earlier studies of Dingle (1980), Dingle et al. (1987), and Dingle and Robson (1992). Seismic Line GeoB/AWI 96-003 (Fig. 3), which runs perpendicular to the continental margin, shows clear evidence for such slumps, particularly in greater water depth. Therefore, the development of a seismostratigraphic concept and its application to all seismic lines in the area is not as straightforward as was expected from the earlier, limited-resolution data of Austin and Uchupi (1982). Near site SCB-1, the sediment column appears to be less disturbed than elsewhere in the region. Although normal faulting of larger blocks is observed and the curved shape of the base faults suggests horizontal displacement and a lack of structural integrity, the sedimentary units at Site 1087 seem to represent mostly undisturbed sections separated by one or more hiatuses.

Figure 3 indicates the location of Sites 1086 and 1087, projected on this profile. Site 1086 is offset from Line GeoB/AWI 96-003 by 22.5 km to the south; Site 1087 by 6 km. The uppermost sedimentary unit of 300 to 400 ms two-way travel time (TWT) thickness is characterized by moderate amplitudes, indicating pelagic deposition. At Site 1087, a stronger reflector marks the transition to seismic Unit 2 of 100 to 150 ms TWT thickness, which reveals higher amplitudes. Within this unit, a major unconformity is observed, which can be identified as a gliding plane of a massive slump event. Sediments are disrupted, and the morphology is significantly disturbed. Seismic Unit 3 of 300 to 400 ms TWT thickness represents the remains after the slump event and is mostly undisturbed, except for some block faulting. Reflectors are of high amplitudes and mostly continuous. The seismic character of the base of this unit at a depth of ~900 ms TWT near Site 1087 is similar to that of DSDP Sites 360 and 361 (Bolli et al., 1978) and is tentatively assigned to Reflector D of Paleocene-Eocene age. Toward the shelf break, the uppermost unit thins out, and it must be assumed that recent sediments have been eroded or not deposited, possibly because of stronger currents in intermediate water masses.

Four additional sites were proposed at the crossings of the seismic lines. None of them allows drilling of a continuous sedimentary section, but the locations of hiatuses and thicknesses are different and allow adjustment to different drilling targets in time and water depth.

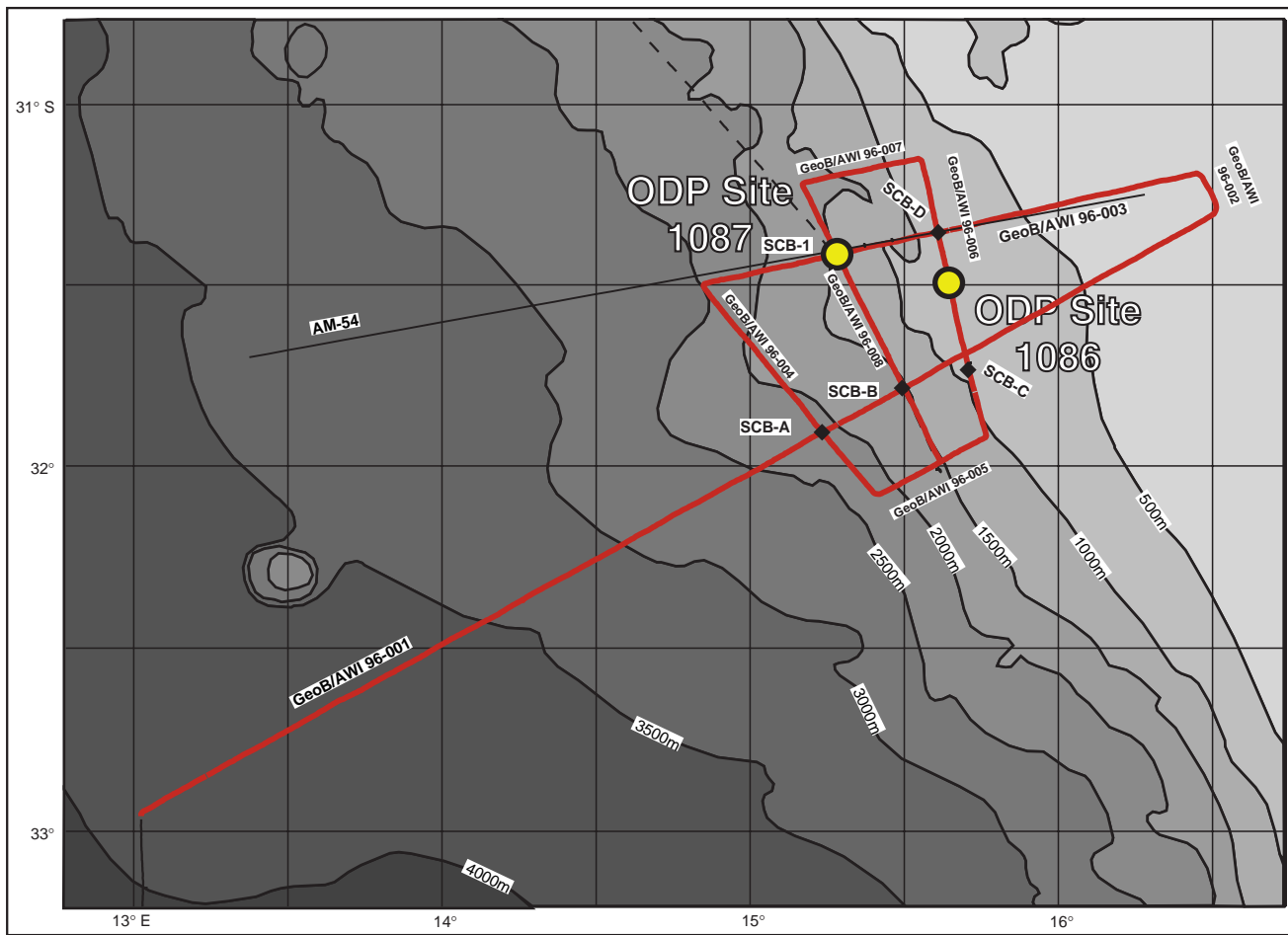


Figure 2. Map of seismic presite survey lines, proposed site locations, and ODP Leg 175 drill Sites 1086 to 1087 in the Southern Cape Basin (SCB). Bathymetry was derived from Gebco Digital Dataset on CD-ROM.

**Site 1086**

Site 1086 is located in 781 m water depth (Fig. 2) on Line GeoB/AWI 96-006 (common depth point [CDP] 1680), 22.5 km south of the crossing with Line GeoB/AWI 96-008. Figure 4 shows a 10-km-long seismic section of Line GeoB/AWI 96-006 across Site 1086. The site was moved from its originally proposed position into shallower water to record signals of intermediate water-mass influence in the area.

The uppermost 400 ms TWT appear mostly undisturbed, although structures in the upper 20 m remain unresolved because of an apparently strong and long seafloor return echo. Beneath 400 ms TWT, a disturbed zone marks the gliding plane of a slump, mentioned above, with sheared sediment blocks. Drilling was therefore limited to a maximum of 250 m.

Figure 5 shows a close-up of the seismic section, plotted against sub-bottom depth for an average sound velocity of 1600 m/s, for a 1-km-long interval near the drill site. Seismic reflectors are compared with the GRAPE density core log (see “Physical Properties” section, this chapter). Although some stronger reflectors can be tentatively correlated with pronounced peaks in the density core log, the seismic signal is not suitable to resolve these fine-scale changes. Seismic returns are therefore a product of interference from closely spaced reflectors, which have to be compared directly with synthetic seismograms to draw further conclusions. Whether the band of reflectors in the uppermost 20 m is an artifact of seismic data acquisition or results from stronger fluctuations of grain size observed in the cores (see “Lithostratigraphy” section, this chapter) must be studied in detail.

**Site 1087**

Site 1087 is located in 1372 m water depth in the middle of the survey area (Fig. 2) on Line GeoB/AWI 96-008 (CDP 1227). Figure 6 shows a 10-km-long seismic section of Line GeoB/AWI 96-008 across Site 1087. This seismic section reveals more details about disturbances at different levels in the sedimentary column (e.g., at 150 and 450 ms TWT), which could not be avoided because of the complex nature of the site area. Although the uppermost unit of 150 ms TWT reveals some lateral variation in thickness, the sediment package from 150 to 450 ms TWT represents pelagic deposition causing continuous reflectors of constant thickness. The interval beneath 450 ms TWT is hummocky with some high-amplitude reflectors, which may suggest a shear zone. Reflector D was tentatively identified at the base of another undisturbed sedimentary unit beneath at 950 ms TWT (see above).

Figure 7 shows a close-up of the seismic section, plotted against sub-bottom depth in TWT, for a 1-km-long interval near the drill site. Seismic reflectors are compared to the GRAPE density core log (see “Physical Properties” section, this chapter). The depth scale of the core log was linearly compressed according to the average sound velocity of 1775 m/s, determined from downhole logging between 80 and 488 mbsf (see “Downhole Logging” section, this chapter). Some reflectors are tentatively correlated to changes in sediment density, but more thorough editing and analyses of both seismic data and core data have to be carried out on shore to relate lithologic changes to seismic reflectors. The rough comparison confirms that the higher seismic amplitudes beneath 430 mbsf are associated with the begin-

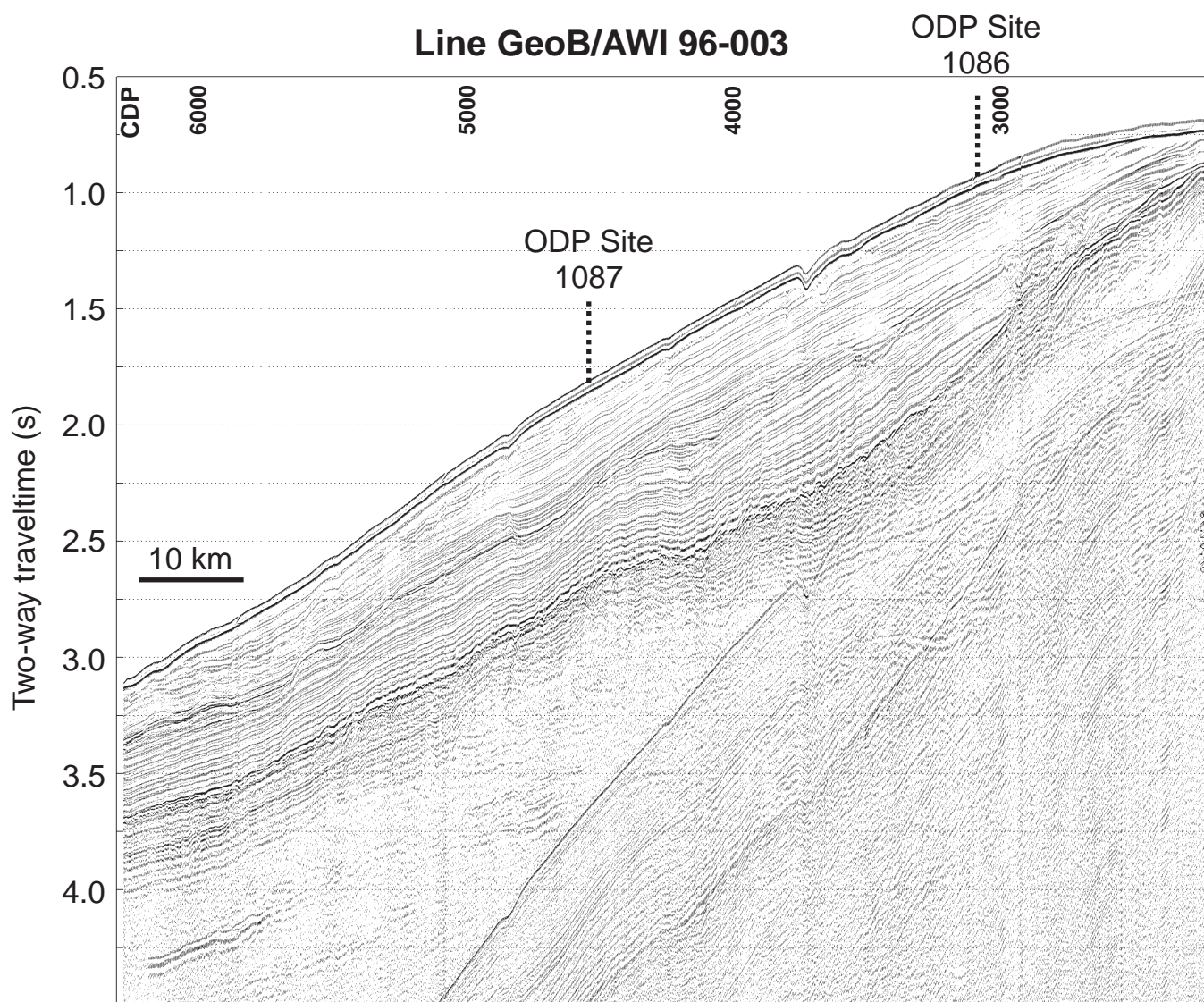


Figure 3. Seismic Line GeoB/AWI 96-003. Sites 1086 and 1087 are projected onto the profile (dashed lines). Vertical axis is given in TWT. CDP interval is 25 m for a shotpoint spacing of 25 m. Seismic data is 24-fold stacked and not migrated.

ning lithification of the sediment, sharp peaks in GRAPE density beyond 2000 kg/m<sup>3</sup>, and the major Miocene/Eocene hiatus.

## LITHOSTRATIGRAPHY

### Description of Lithostratigraphic Unit

The sediment drilled at Site 1086 exhibited only minor core disturbance resulting from gas expansion. Drilling disturbance was evident in the upper seven cores of Hole 1086A, whereas the core quality was significantly better at Hole 1086B. No flow-in structures were observed. Sediments from Site 1086 form one lithostratigraphic unit and are composed of olive (5Y 5/3) clay-rich nannofossil-foraminifer ooze and olive (5Y 5/3), light gray (5Y 7/1), pale olive (5Y 6/3) and light olive-gray (5Y 6/2) foraminifer-nannofossil ooze, foraminifer-rich nannofossil ooze, and nannofossil ooze.

#### Unit I

Intervals: 175-1086A-1H through 175-1086A-22H; 175-1086B-1H through 175-1086B-23H  
Age: early Pleistocene to late Miocene  
Depth: Hole A: 0–206.2 mbsf; Hole B: 0–208.3 mbsf

Unit I is composed of olive (5Y 5/3) clay-rich nannofossil-foraminifer ooze and olive (5Y 5/3), light gray (5Y 7/1), pale olive (5Y 6/3) and light olive-gray (5Y 6/2) foraminifer-nannofossil ooze, foraminifer-rich nannofossil ooze, and nannofossil ooze (Fig. 8). Most of the sediment is moderately bioturbated, and burrows range in diameter from 1 mm to over 1 cm. Thicker burrows are dark gray, contain abundant pyrite, and are frequently infilled with coarser sediment consisting of abundant foraminifer tests in a nannofossil-ooze matrix. Occasionally, *Zoophycos* traces are identified (e.g., Core 175-1086A-17H-6). Intervals of different colored sediment range in thickness from 40 to 100 cm and grade into one another over 15 to 20 cm. Small, finely dispersed fine sand-sized pyrite grains are ubiquitous below Core 175-1086A-16H. Calcium carbonate content at Hole 1086A averages 79 wt%.

Cores 175-1086A-1H through 4H and 175-1086B-1H through 3H contain nannofossil-rich foraminifer ooze with an increasing abundance of nannofossils downhole. These cores have little or no clay or silt fraction, except in Core 175-1086A-1H where silt-sized grains of quartz are frequent. Below these cores, the sediment is primarily either a foraminifer-rich nannofossil ooze or a nannofossil-foraminifer ooze. Egg-shaped carbonate concretions ~3 to 5 cm in diameter are present in Cores 175-1086A-16H and 19H. Bioturbated 1-cm-

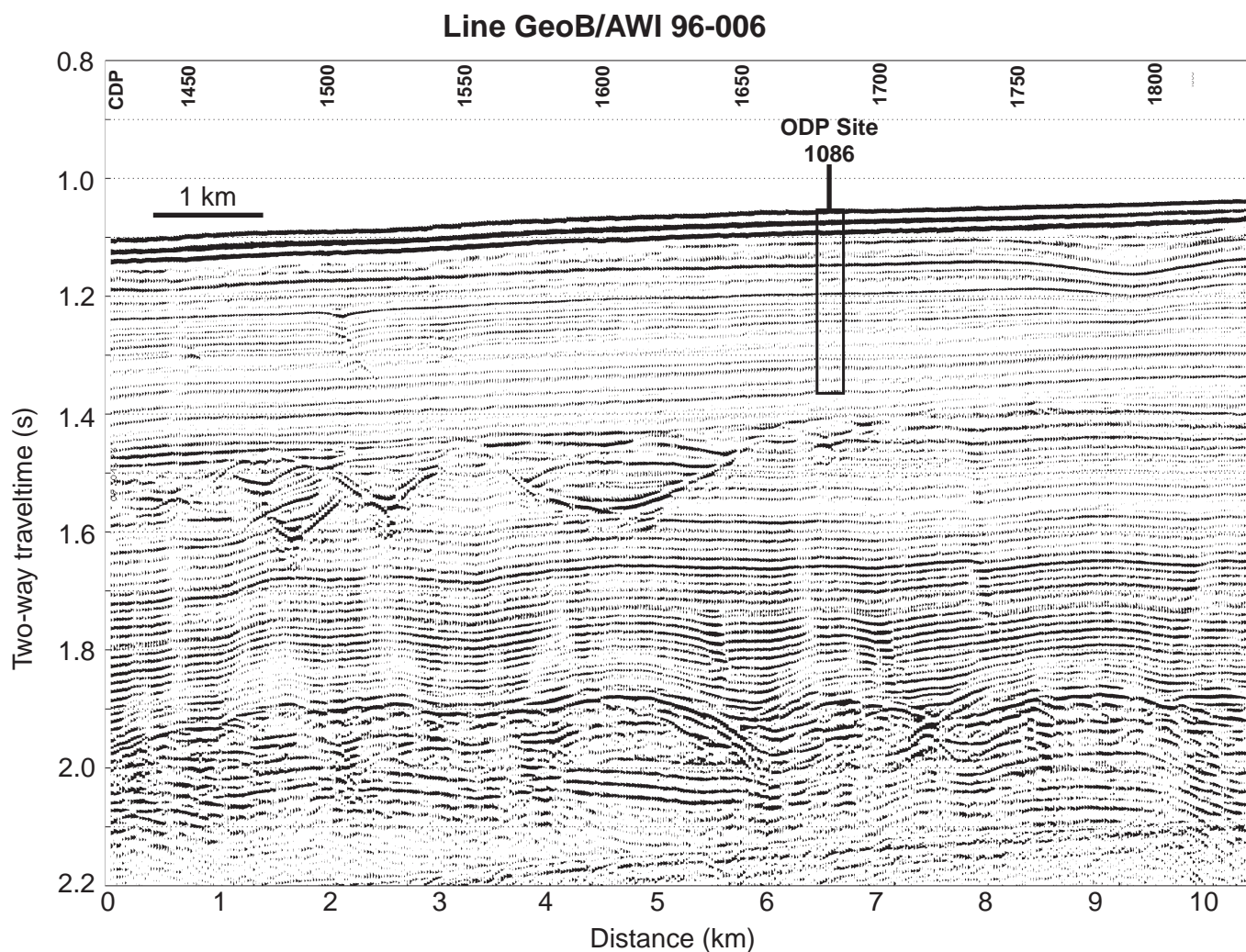


Figure 4. Seismic section of Line GeoB/AWI 96-006 at Site 1086. Vertical axis is given in TWT. CDP interval is 25 m for a shotpoint spacing of 25 m. Site 1086 is located at CDP 1680. The box indicates the approximate penetration of the borehole of 200 m.

thick beds composed of very fine-grained, subrounded phosphate grains are present in Sections 175-1086A-11H-1, 134 cm, and 11H-6, 87 cm. A 2-mm-thick lamina composed of very fine-grained, subangular phosphate grains is also present in Section 175-1086B-13H-5, 144 cm.

### Synthesis of Smear-Slide Analyses

The detrital component in sediments from Site 1086A is dominated by clay and trace abundances of silt-sized, subangular mono- and polycrystalline quartz grains. Authigenic minerals are rare or present in trace abundances. Pyrite is present as silt-sized aggregates of euhedral crystals or as framboids. Small phosphate grains are present in bioturbated beds in Core 175-1086A-11H and in a 2-mm-thick lamina in Core 175-1086B-13H. The biogenic component in all smear slides consists of abundant to dominant nanofossils and abundant to common foraminifers.

### Spectrophotometry

Color reflectance data were measured every 4 cm for Holes 1086A and 1086B. The total reflectance values range between 35% and 70% (Fig. 9). High average calcium carbonate contents at this site (see "Organic Geochemistry" section, this chapter) suggest that downcore variations in the total reflectance are controlled primarily

by variations in calcium carbonate. At Hole 1086A, total reflectance values are, on average, 55% for the first 150 mbsf and show relatively high-amplitude variations between 70 and 150 mbsf (Fig. 9). Between 150 mbsf and the bottom of Hole 1086A, total reflectance values average 65%. Downcore stratigraphic trends of total reflectance as well as specific features are similar at Sites 1086 and 1085.

### BIOSTRATIGRAPHY AND SEDIMENTATION RATES

Sediments recovered from Site 1086 represent a continuous pelagic section spanning the upper Miocene to lower Pleistocene. The biostratigraphic framework developed for Site 1086 was based on calcareous microfossils. Siliceous microfossils are rare or absent in much of the core. There is generally good agreement between stratigraphic position of the calcareous nanofossil and planktonic foraminiferal datums and between the biostratigraphic and magnetostratigraphic age model (see "Paleomagnetism" section, this chapter). The superior quality of the paleomagnetic data for Site 1086 allowed us to examine in detail the differences in time scales in the early Pliocene.

A comparison of the calcareous nanofossil-based age model for this interval with an age model generated from paleomagnetic data indicates a significant offset in the timing of changes in sedimentation rates. The biostratigraphic age model based on the Lourens et al.

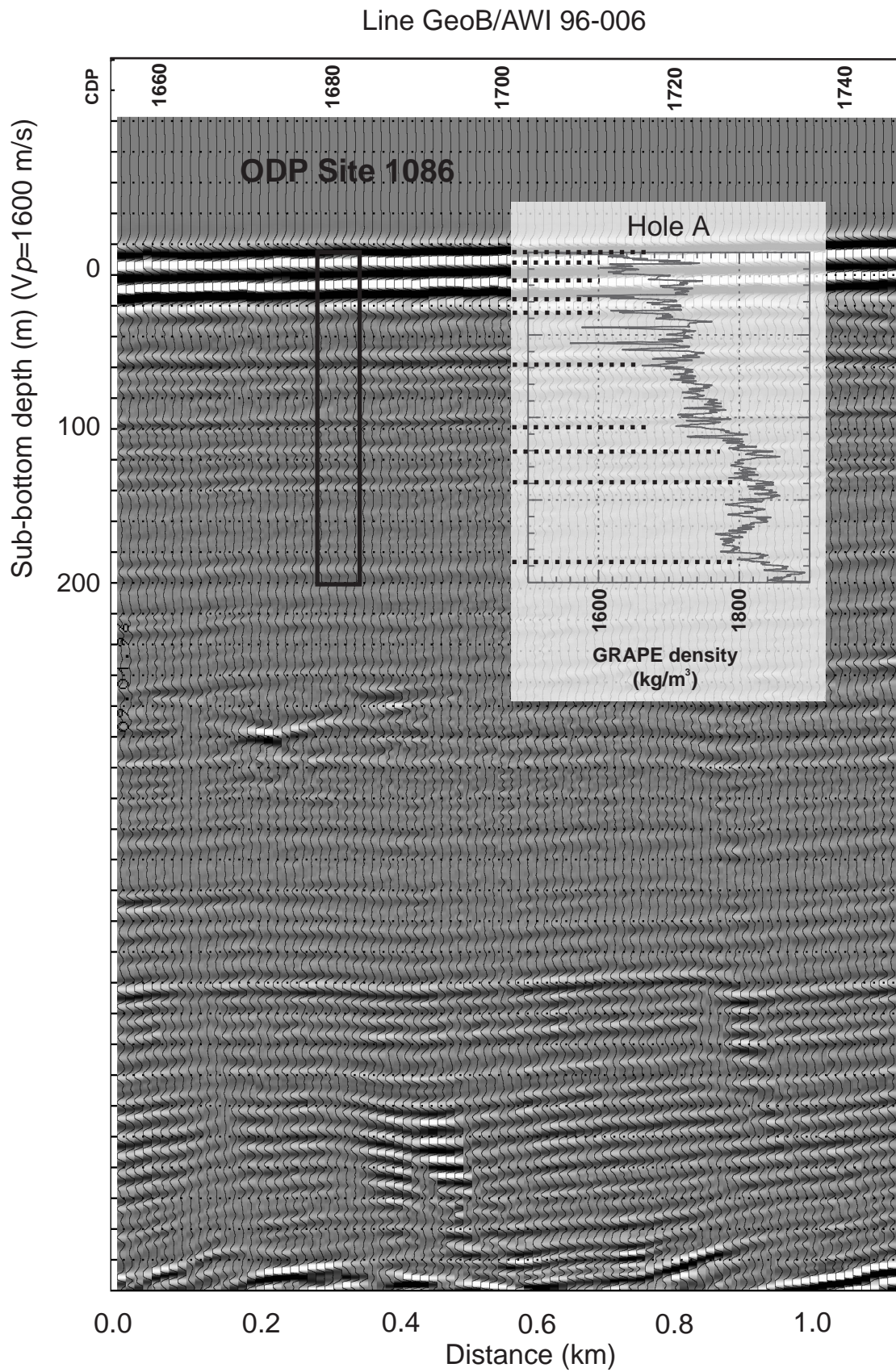


Figure 5. Close-up of Line GeoB/AWI 96-006 near Site 1086. Amplitudes are grayscale. For comparison, GRAPE density data from MST measurements are shown. Many peaks may be associated with seismic reflectors (thick dashed lines). For depth determination, an average sound velocity ( $V_p$ ) of 1600 m/s was used.

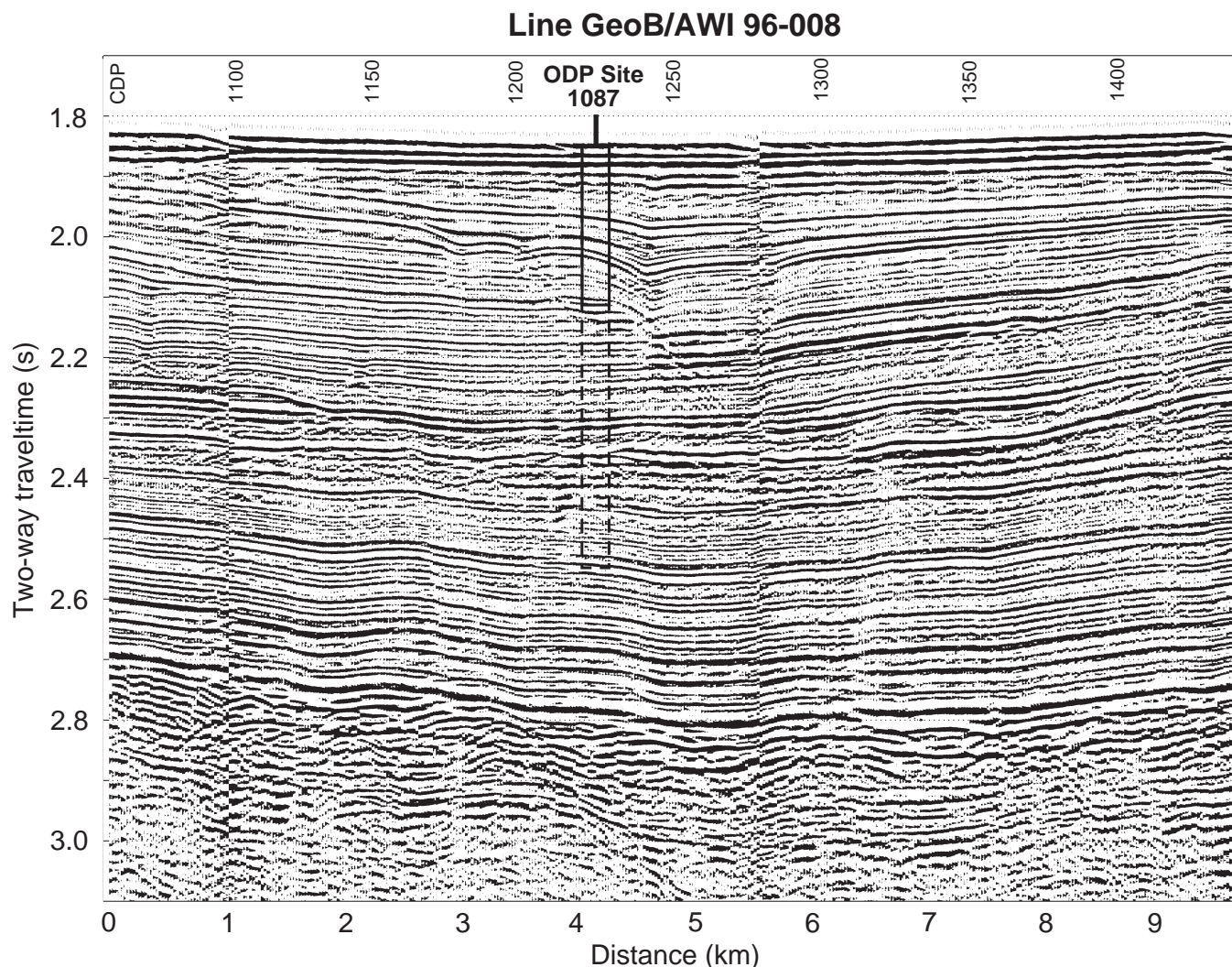


Figure 6. Seismic section of Line GeoB/AWI 96-008 at Site 1087. Vertical axis is given in TWT. CDP interval is 25 m for a shotpoint spacing of 25 m. Site 1087 is located at CDP 1227. The box indicates the approximate penetration of the borehole of at 200 (APC) and 500 m (XCB), respectively.

(1996) time scale produces an increase in sedimentation rate that occurs 0.7 m.y. earlier than the one produced by the Berggren et al. (1995) paleomagnetic age model. There are known problems associated with the radiometric dating in Chron C3n (4.2–5.2 Ma; Berggren et al., 1995). The Berggren et al. (1995) time scale lacks high precision  $^{40}\text{Ar}/^{39}\text{Ar}$  dating in Chron C3n. The Lourens et al. (1996) time scale represents an improvement to the Berggren et al. (1995) time scale for this interval because it integrates radiometric dating and astronomical tuning.

This deviation in the early Pliocene was not detected at other sites during Leg 175 because of lower sedimentation rates, lower quality paleomagnetic data, and/or carbonate dissolution.

### Calcareous Nannofossils

Calcareous nannofossils were studied in core-catcher samples from Hole 1086A. Because additional samples from within the cores were not examined, the depth range of the datum events identified at Site 1086 is approximately  $\pm 5$  m. Nannofossils are abundant and well preserved throughout the entire section.

Based on the oldest identified datum (last occurrence [LO] of *Amaurolithus primus*; 7.2 Ma) as well as paleomagnetic data (see “Paleomagnetism” section, this chapter), Site 1086 terminated within Zone NN11 (late Miocene). The top core of Hole 1086A probably

does not contain material younger than 1.25 Ma, as shown by the presence within Sample 175-1086A-1H-CC of *Helicosphaera sellii*, a species whose LO event is dated at 1.25 Ma. Of the 10 biohorizons identified within Hole 1086A, six are zonal boundary markers (Table 2). Within the sampling resolution, the sedimentation appears continuous throughout the entire section (Fig. 10). The nannofossil-derived biostratigraphy agrees with the magnetostratigraphy derived from this site (see “Paleomagnetism” section, this chapter), except between 3.8 and 5.5 Ma (early Pliocene), as discussed above.

### Zone NN19

The top 21 mbsf of Hole 1086 are placed within Zone NN19. Consequently, drilling at Site 1086 did not recover any late Pleistocene material. Based on sedimentation rate estimates (Fig. 10), the Pleistocene/Pliocene boundary can be placed at  $\sim 15$  mbsf.

### Zones NN18–NN17

The top of Zone NN18 is defined by the LO of *Discoaster brouweri*, a datum event recognized between Samples 175-1086A-2H-CC and 3H-CC. Zones NN18 and NN17 were lumped together because the LOs of both *D. pentaradiatus* (NN18/NN17 zonal boundary event) and *D. surculus* (NN17/NN16 zonal boundary) were identified

## Line GeoB/AWI 96-008

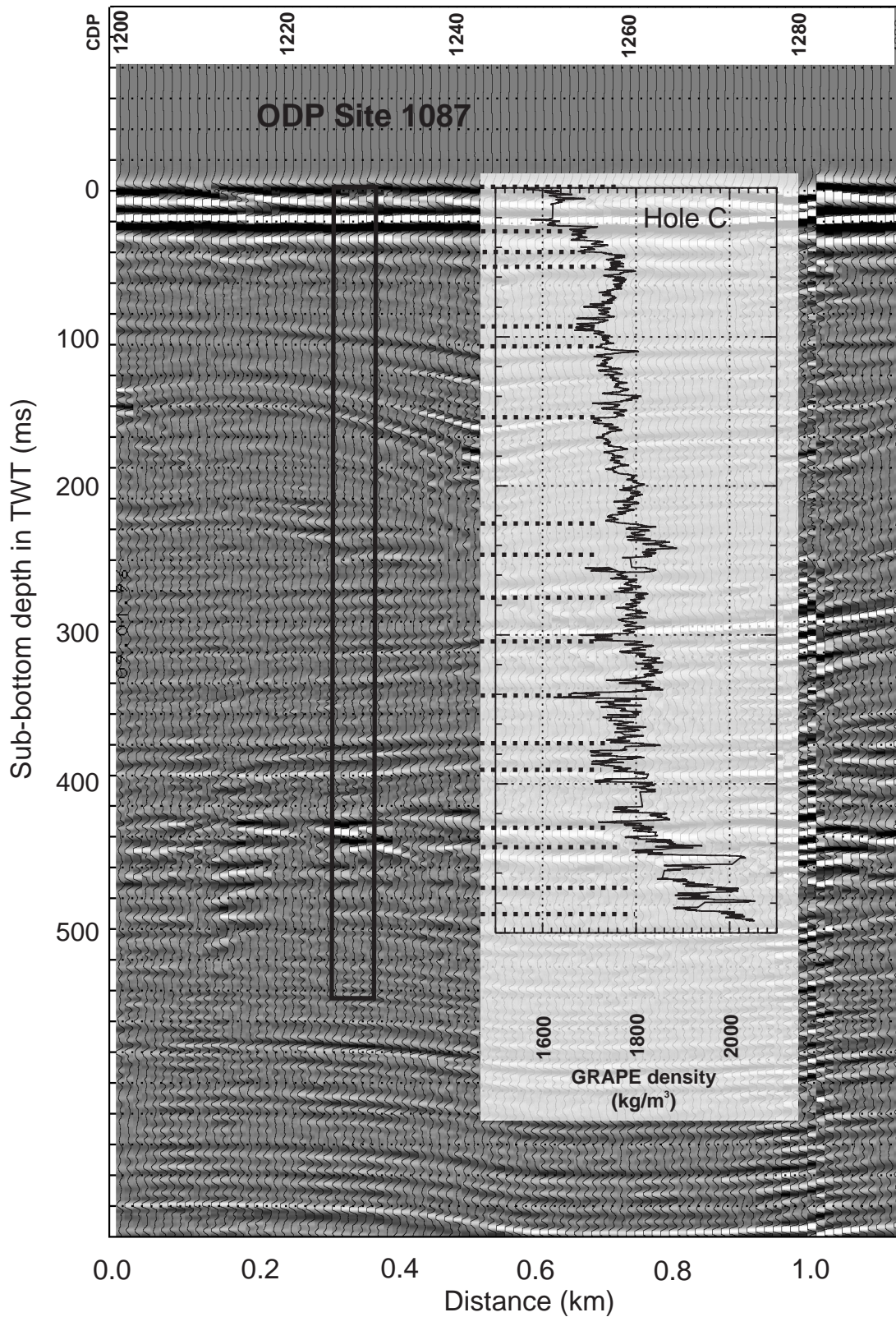


Figure 7. Close-up of Line GeoB/AWI 96-008 near Site 1087. Vertical axis is given in TWT Amplitudes are grayscale. For comparison, the GRAPE density profile from MST measurements is shown. Depth scale is transferred to the TWT scale using the average sound velocity of 1775 m/s, derived from downhole logging. Selected reflectors can be tentatively correlated with local extremes in the core log (thick dashed lines).

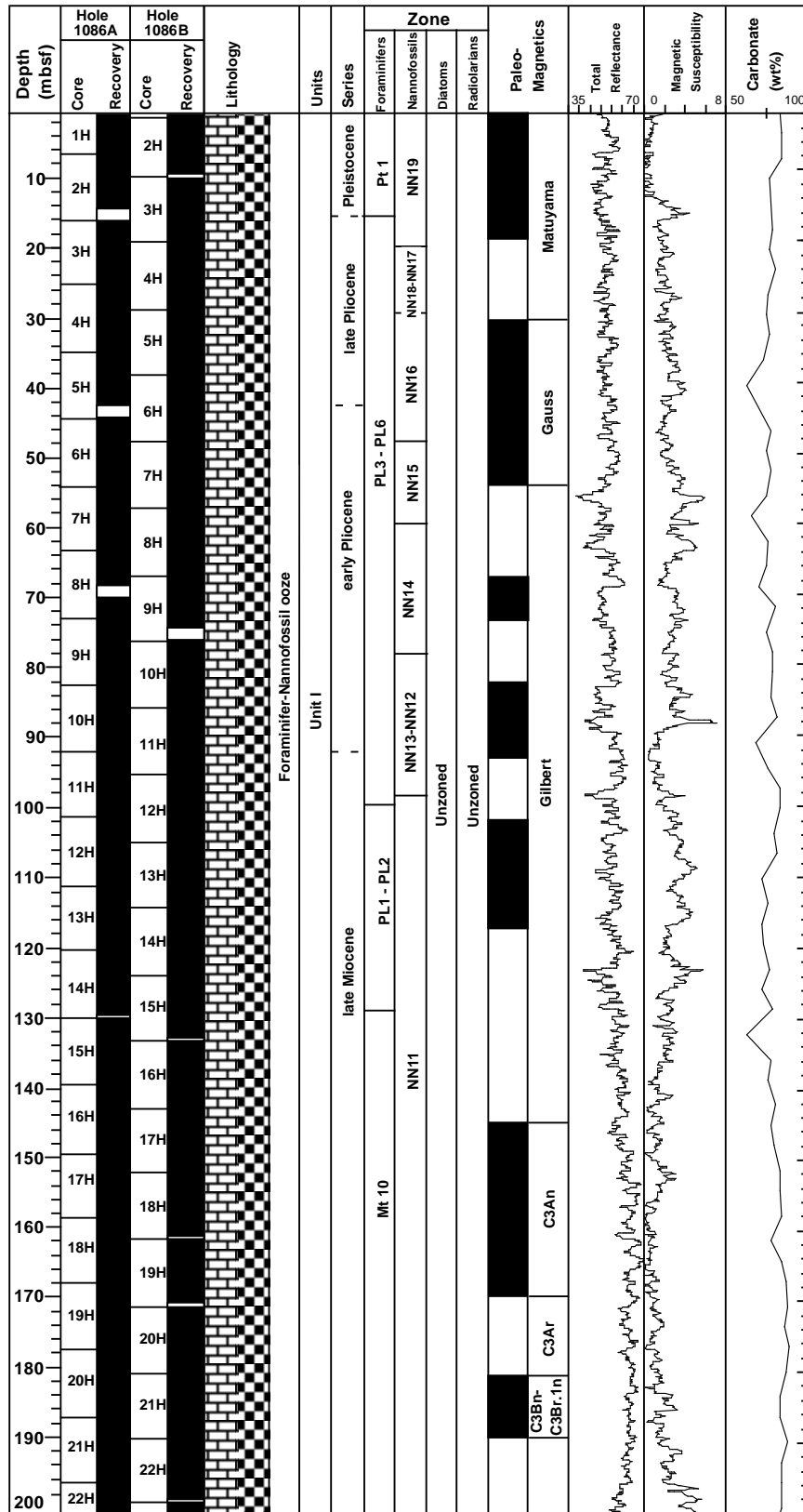


Figure 8. Composite stratigraphic section for Site 1086 showing core recovery in all holes, a simplified summary of lithology, age, total reflectance (400–700 nm), magnetic susceptibility, and calcium carbonate.

within the same sampling interval. The base of Zone NN17 was identified between Samples 3H-CC and 4H-CC at the mean depth of 30.9 mbsf.

### Zone NN16

This interval is constrained between 30.9 and 48.9 mbsf. *Discoaster brouweri*, *D. pentaradiatus*, and *D. surculus* are the only star-shaped coccoliths identified within this sequence at Hole 1086A. The diagnostic species for the lower part of Zone NN16 (Subzone CN12a), *D. tamalis*, *D. variabilis*, and *D. challengerii*, are missing from the investigated samples, pointing either to a condensed CN12a interval, or an overall low diversity of *Discoaster* specimen because of cool surface-water conditions.

### Zone NN15

The top of this interval is defined by the LO of *Reticulofenestra pseudoumbilica* (3.82 Ma), a datum event identified between Samples 175-1086A-5H-CC and 6H-CC. This interval is marked by the

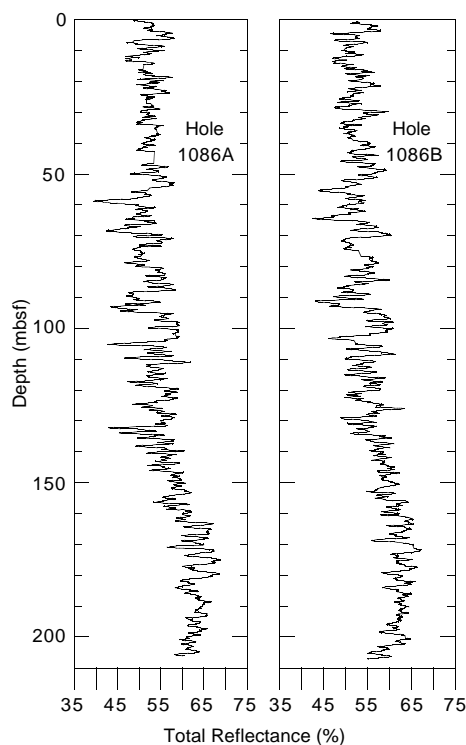


Figure 9. Downcore variations in the total reflectance at Holes 1086A and 1086B.

first downhole occurrence of *Sphenolithus* sp. The Zone NN15/NN14 boundary is defined by the LO of *Amaurolithus tricorniculatus* (4.5 Ma), a datum identified at the mean depth of 59.4 mbsf (Samples 6H-CC through 25H-CC).

### Zone NN14

The base of this 0.52-m.y. interval was identified between Samples 175-1085A-26H-CC and 27H-CC (first occurrence [FO] of *Discoaster asymmetricus*; 5.02 Ma).

### Zones NN13–NN12

This interval is constrained between the mean depths of 78.3 and 97.3 mbsf. Zone NN13 is lumped together with Zone NN12 because of the sparse occurrence of *Ceratolithus* spp. throughout this interval. The LO of *Discoaster quinquerramus* (5.54 Ma), identified between Samples 175-1086A-10H-CC and 11H-CC, defines the NN12/NN11 zonal boundary.

### Zone NN11

This 3.06-m.y. interval is defined as the range of *D. quinquerramus*. The range of *Amaurolithus amplificus* (LO between Samples 175-1086A-15H-CC and 16H-CC; FO between Samples 175-1086A-17H-CC and 18H-CC) and the LO of *Amaurolithus primus* (7.2 Ma) were used to refine the age model.

## Planktonic Foraminifers

### Pleistocene

The top two samples (175-1086A-1H-CC and 2H-CC) are assigned to Pleistocene Zone Pt1 (1.77–0 Ma). Zone Pt1 was not differentiated, although Sample 1H-CC (6.72 mbsf) is older than 0.65 Ma, based on the presence of *G. tosaensis*. The presence of *G. crassaformis viola* (latest Pliocene to early Pleistocene) corroborates the age. Sample 1H-1, 19–21 cm was examined, but no upper Pleistocene foraminifers were found in the core top. The base of Zone Pt1 is placed at 12 mbsf, based on the LO of *G. truncatulinooides* in Sample 2H-CC (Table 3).

### Pliocene

Zonation was difficult in the Pliocene because many of the marker species are present only sporadically or are dissolution susceptible. For example, *Globorotalia margaritae* (last-appearance datum [LAD] at 3.58 Ma) is a diagnostic index fossil for the early Pliocene and is present from 97.4 to 135 mbsf (Samples 175-1086A-11H-CC through 14H-CC). The paleomagnetic and calcareous nannofossil data, however, indicate that the top of the lower Pliocene sequence occurs high-

Table 2. Calcareous nannofossil datums at Hole 1086A.

Event	Age (Ma)	Zone (base)		Core, section, interval		Depth (mbsf)		
		A	B	Top	Bottom	Top	Bottom	Mean
LO <i>Calcidiscus macintyrei</i>	1.67			175-1086A-1H-CC	175-1086A-2H-CC	6.72	16.00	11.36
LO <i>Discoaster brouweri</i>	1.95	NN19	CN13a	2H-CC	3H-CC	16.00	26.15	21.08
LO <i>Discoaster surculus</i>	2.55	NN17	CN12c	3H-CC	4H-CC	26.15	35.65	30.90
LO <i>Reticulofenestra pseudoumbilica</i>	3.82	NN16	CN12a	5H-CC	6H-CC	43.10	54.67	48.89
LO <i>Amaurolithus tricorniculatus</i>	4.5	NN15	CN11	6H-CC	7H-CC	54.67	64.16	59.42
FO <i>Discoaster asymmetricus</i>	5.02	NN14	CN10d	8H-CC	9H-CC	73.59	83.05	78.32
LO <i>Discoaster quinquerramus</i>	5.54	NN12	CN10a	10H-CC	11H-CC	92.66	102.05	97.36
LO <i>Amaurolithus amplificus</i>	5.9			15H-CC	16H-CC	140.04	149.73	144.89
FO <i>Amaurolithus amplificus</i>	6.6			17H-CC	18H-CC	159.10	168.59	163.85
FO <i>Amaurolithus primus</i>	7.2			20H-CC	21H-CC	187.66	197.04	192.35

Notes: FO = first occurrence and LO = last occurrence. Zonal codes are those from (A) Martini (1971) and (B) Okada and Bukry (1980).

er up in the section at ~ 60 mbsf. Although *G. margaritae* is present in temperate regions, it is a dissolution-susceptible species (Bulli and Saunders, 1985), and so its anomalous occurrence at Site 1086 is attributed to dissolution. Paleogeographic changes as well as dissolution affect the distribution of the species downcore. For example, *S. seminulina* (LAD at 3.12 Ma) and *D. altispira* (LAD at 3.09 Ma) have premature LOs at this site, some ~50 m lower in the section than the nannofossil and paleomagnetic age models predict (Fig. 10). Both of these species are tropical to subtropical species (Kennett and Srinivasan, 1983), and this may indicate a cooling in the surface waters at that time (late Miocene to early Pliocene).

The late Pliocene Zones P6–P3 (97–12 mbsf) could not be differentiated (Samples 175-1086A-3H-CC through 7H-CC). The early Pliocene (135–97.4 mbsf) is identified by the presence of *G. margaritae* (Samples 175-1086A-11H-CC through 14H-CC). Zones P12 and P11 are not differentiated because the boundary is the LAD of *G. nepenthes*, a species that is not present in this interval. The top of earliest Pliocene Zone PL1a is defined on the LO of *G. ciboensis* (Sample 12H-CC) at 116 mbsf, although *G. ciboensis* is rare in these samples. *G. juanai* ranges through the lowermost part of P11a (Zone N18 of Blow, 1969), and the LO of *G. juanai* in Sample 11H-CC (106.8 mbsf) therefore restricts that interval to the lowermost Pliocene. This is in agreement with calcareous nannofossil datums and suggests that the top of Zone P11a should be moved up stratigraphically. The base of Zone P11 is placed at 135 mbsf and is coeval with the FO of *G. sphericomiozea* (5.6 Ma; Sample 14H-CC).

The Miocene transitional Zone Mt10 ranges from Samples 175-1086A-15H-CC through 22H-CC (the base of the core), based on the presence of *G. conomiozea* (FAD at 6.9 Ma) in Sample 22H-CC and the absence of *G. sphericomiozea*. (FO at 5.6 Ma) in Samples 15H-CC and 16H-CC. The absence of temperate to warm subtropical

(Kennett and Srinivasan, 1983) species *G. sphericomiozea* in Samples 15H-CC (140 mbsf) and 16H-CC (149.73 mbsf) may be caused by ecological forcing.

### Benthic Foraminifers

Benthic foraminifers are abundant throughout Hole 1086A, but as at Site 1085, there is a very high planktonic to benthic ratio. The preservation of the benthic foraminiferal assemblages is good throughout Hole 1086A (Table 4).

The uppermost core catcher (Sample 175-1086A-1H-CC; 6.72 mbsf) is dominated by *Cassidulina laevigata* and *Trifarina bradyi*. The presence of *Uvigerina spinulosa* in this sample confirms an early Pleistocene age because this species only persists into the earliest Pleistocene (Boersma, 1984).

The core catchers in the Pliocene part of Hole 1086 (Samples 175-1086A-3H-CC through 13H-CC; 26.15–120.86 mbsf) are dominated by *Cibicides pachyderma*, *Stilostomella* spp., and *Uvigerina auberiana* and, in the lower part of this interval, *T. bradyi*. Samples from the early Pliocene and the uppermost late Miocene contain high abundances of *Uvigerina hispida*.

Studied samples from the late Miocene (Samples 175-1086A-15H-CC through 21H-CC; 140.04–197.04 mbsf) contain mostly similar species as the subsequent Pliocene interval, but with the addition of high percentages of *Cibicides bradyi*, which at Hole 1086A is restricted to the late Miocene.

### Radiolarians

Radiolarians are absent or extremely rare (one specimen per sample) in all core-catcher samples from Hole 1086A, except for Sample

Figure 10. Age-depth plot and sedimentation rates estimated from calcareous microfossil datums at Hole 1086A. F = planktonic foraminifers and N = calcareous nannofossils.

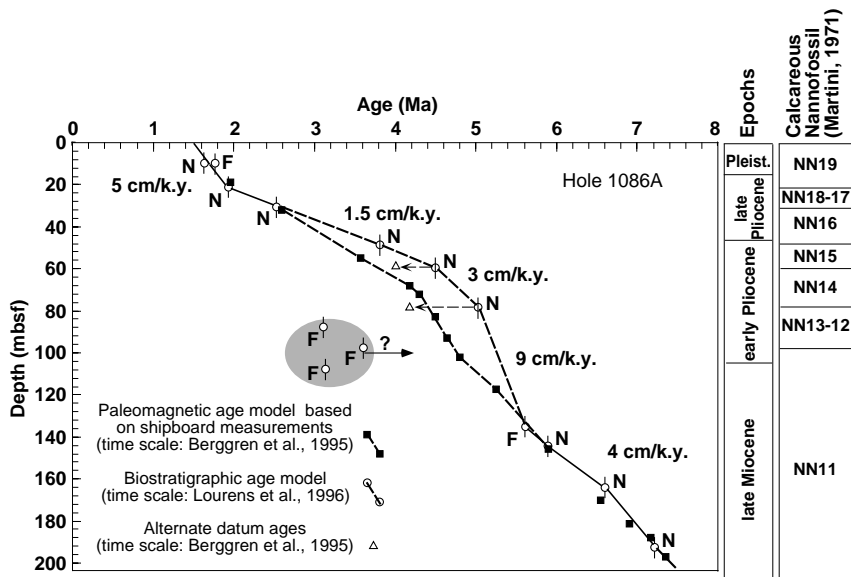


Table 3. Planktonic foraminiferal datums at Hole 1086A.

Event	Age (Ma)	Zone	Core, section, interval		Depth (mbsf)		
			Top	Bottom	Top	Bottom	Mean
LO <i>Globorotalia tosaensis</i>	0.65	Pt1b bottom	175-1086A-1H-0-0	175-1086A-1H-CC	0.00	6.72	3.36
FO <i>Globorotalia truncatulinoides</i>	1.77	Pt1a bottom	2H-CC	3H-CC	6.72	~16.00	12.00
LO <i>Dentoglobigerina altispira</i>	3.09	P14 top	9H-CC	10H-CC	83.05	92.66	87.86
LO <i>Sphaeroidinellopsis</i> spp.	3.12	P13 top	11H-CC	12H-CC	102.05	111.54	106.80
LO <i>Globorotalia margaritae</i>	3.58	P12 top	10H-CC	11H-CC	92.66	102.05	97.36
FO <i>Globorotalia sphericomiozea</i>	5.6		14H-CC	15H-CC	129.93	140.04	134.99
FO <i>Globorotalia conomiozea</i>	6.9	MT10 bottom	22H-CC		206.56		

Note: FO = first occurrence and LO = last occurrence.



175-1086A3H-CC, which yielded rare and poorly preserved radiolarians. The radiolarian assemblage from Sample 3H-CC, characterized by spherical spumellarians, *Axoprunum stauraxonium*, and the *Ellipsoxiphus attractus* group, suggests a warm and low productivity oceanographic condition. No age indicator species nor reworked specimens were identified.

### Diatoms

Smear slides and the 63- $\mu\text{m}$ -sieved fraction of each core-catcher sample from Hole 1086A were analyzed for their diatom content. Diatoms are absent or extremely rare (one *Coscinodiscus* specimen in Sample 175-1086A-5H-CC, and another one in Sample 11H-CC in the sieved fraction) at Hole 1086A. Silicoflagellates are absent. Sponge spicules are present in Samples 175-1086A-2H-CC through 4H-CC only; they are particularly abundant in Sample 3H-CC (26.15 mbsf; ~1.95 Ma).

As was the case at Site 1085, dinoflagellate cysts are also present at Site 1086; abundances range from frequent to common in Samples 175-1086A-15H-CC (140.04 mbsf) through the end of the hole (206.56 mbsf). It is interesting to note that the age of the LO of dinoflagellate cysts at Site 1086 approximates that of Site 1085 (~5.8 Ma), suggesting that both sites were affected by the same oceanographic process simultaneously.

## PALEOMAGNETISM

The investigation of magnetic properties at Site 1086 included the measurement of magnetic susceptibility of whole-core sections and the natural remanent magnetization (NRM) of archive-half sections. The Tensor tool was used to orient Cores 175-1086A-3H, 4H, 5H, 21H, and 22H, 175-1086B-4H through 23H, except for 12H (Table 5). Cores 175-1086A-6H through 20H were not oriented because of technical problems with the Tensor tool.

### Natural Remanent Magnetization and Magnetic Susceptibility

Measurements of NRM were made on all archive-half core sections from Holes 1086A and 1086B. All sections were demagnetized by AF at 20 mT. Magnetic susceptibility measurements were made on whole cores from all holes as part of the MST analysis (see "Physical Properties" section, this chapter).

The intensity of NRM after 20-mT demagnetization is between  $\sim 10^{-3}$  and  $10^{-5}$  A/m, and magnetic susceptibility ranges between 0 and  $3 \times 10^{-5}$  (SI volume units). In general, these two properties show parallel variations.

Except for the uppermost ~30 mbsf, the cores show significant coring-induced magnetization (CIM) with a radial-inward direction (see "Paleomagnetism" section, "Site 1077" and "Site 1081" chapters, this volume). The CIM is evident from the clustering of declinations around  $0^\circ$  before orientation. In contrast, inclinations showed distinct polarity biases after 20-mT demagnetization, from which an interpretation of the magnetic polarity was possible.

### Magnetostratigraphy

We identified the polarity of the NRM mainly from the inclinations (Fig. 11). Considering constraints from the biostratigraphy (see "Biostratigraphy and Sedimentation Rates" section, this chapter), we interpreted the observed polarity reversal sequence from Chrons C2n (Olduvai Subchron) to C4n (~7.5 Ma; Berggren et al., 1995). Magnetostratigraphic interpretation is summarized in Table 6. Figure 12 displays the relation between depth below seafloor and age. The sedimentation rate dropped from ~40 to 25 m/m.y. at ~4 Ma. Sediments of Pleistocene age are very thin, 15 m or less, within which we could

**Table 5. Tensor tool-orientation data for cores from Holes 1086A and 1086B.**

Core	MTF ( $^\circ$ )	Inclination angle
175-1086A-		
3H	179	1.17
4H	325	1.39
5H	342	1.32
21H	312	0.47
22H	224	0.48
175-1086B-		
4H	63	0.46
5H	159	0.48
6H	65	0.95
7H	241	0.43
8H	270	0.56
9H	321	0.34
10H	234	1.08
11H	335	0.41
13H	54	0.59
14H	66	0.67
15H	57	0.62
16H	103	0.70
17H	106	0.33
18H	26	0.30
19H	160	0.21
20H	36	0.47
21H	9	0.46
22H	107	0.34
23H	147	0.38

Notes: The orientation parameter (MTF) is the angle in degrees between magnetic north and the double line marked on the center of the working half of the core. The local declination anomaly is  $21^\circ\text{W}$ .

not obtain a good magnetostratigraphy, partly because of physical disturbance of the surface sediments.

## COMPOSITE SECTION

At Site 1086, two holes were cored with the APC corer to a maximum depth of 206 mbsf. Measurements of magnetic susceptibility and GRAPE density were made on the MST, and color reflectance was measured with the Minolta spectrophotometer. All parameters were measured at 10-cm resolution. Graphic and quantitative alignment of stratigraphic features of the MST and color reflectance data were used to depth adjust adjacent cores to establish a meters composite depth (mcd) scale. Beginning from the core top, a constant was added to the mbsf scale to establish depth offsets for each core to assemble a single continuous composite section. For Site 1086, continuity of the composite section was demonstrated to 232 mcd, covering the entire depth cored.

Magnetic susceptibility, GRAPE, and color reflectance (lightness  $L^*$ ) data were all used to construct a composite section and to verify core gaps. Total reflectance was the primary parameter used to constrain intercore depth adjustments; however, all parameters were useful in establishing continuity. A 31-cm Gaussian filter was used to smooth all parameters in the composite section.

The composite depth section shows excellent agreement between Holes 1086A and 1086B (Fig. 13). Depth offsets for individual cores relative to their mbsf position are given in Table 7. Intracore stretching and compression often lead to feature mismatches of the data, which are indicative of core distortion and cannot be resolved with a single depth adjustment per core. Splices at 47 and 216 mcd are based upon limited overlap; however, the offsets are consistent with core expansion, suggesting that if gaps exist, they are relatively small (<1 m). The composite section over these intervals should be regarded with caution.

Upon completion of the composite depth sections, a single spliced record was assembled using overlapping cores from Holes 1086A and 1086B for magnetic susceptibility and lightness ( $L^*$ ; Fig. 14). Hole 1086A served as the backbone of the sampling splice. The

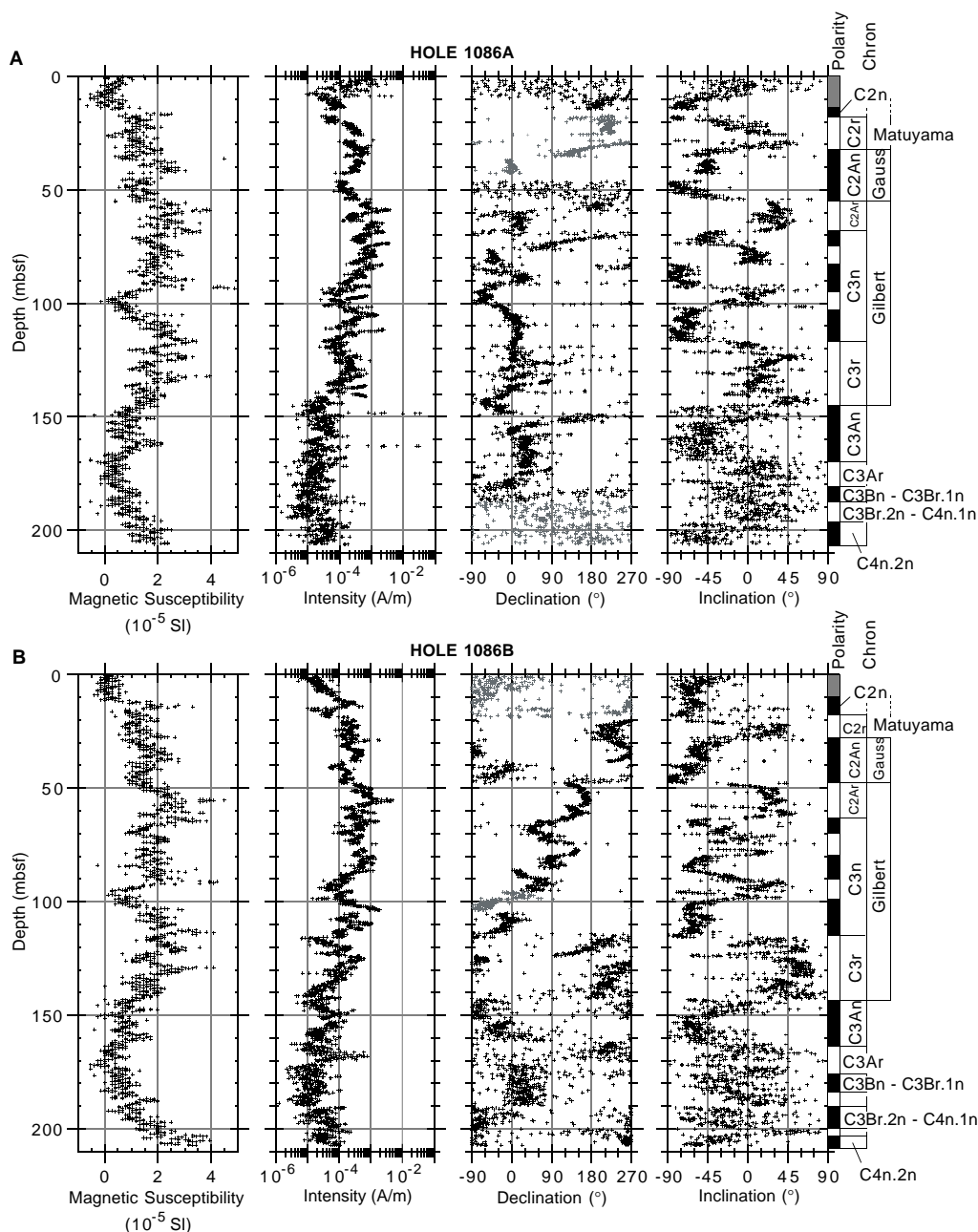


Figure 11. Magnetic susceptibility (SI volume units) and NRM intensity, declination, inclination, and magnetostratigraphic interpretation after 20-mT demagnetization for (A) Hole 1086A and (B) Hole 1086B. Black symbols = Tensor corrected; gray symbols = uncorrected. Polarity shading: black = normal, white = reversed, and gray = ambiguous.

Table 6. Magnetostratigraphic interpretations for Site 1086.

Polarity chron	Age (Ma)	Depth (mbsf)		Polarity epoch
		Hole 1086A	Hole 1086B	
C2n (bottom)	1.95	19	19	Olduvai
C2An.1n (top)	2.58	32	28	Gauss
C2Ar (top)	3.58	55	49	Gilbert
C3n.1n	4.18-4.29	68-74	63-70	Cochiti
C3n.2n	4.48-4.62	83-93	80-90	Nunivak
C3n.3n-4n	4.80-5.23	102-117	99-114	Sidufjall-Thvera
C3An (top)	5.89	145	143	
C3Ar (top)	6.56	170	164	
C3Bn - C3Br.1n	6.94-7.17	181-188	176-184	
C3Br.2n - C4n.1n	7.34-7.56	197	190-200	
C4n.2n (top)	7.65	—	203	

Note: Time scale used is that of Berggren et al. (1995).

splice for Site 1086 (Table 8) can be used as a sampling guide. Core expansion relative to the mbsf scale is ~10% (Fig. 15).

## INORGANIC GEOCHEMISTRY

Sixteen interstitial water samples were gathered from Hole 1086A between 1.4 and 201.1 mbsf. Whole-round samples were sampled at a frequency of one sample per core to 96.6 mbsf and every third core thereafter to total depth (Table 9). As was the case at Site 1085, also located in the Cape Basin, the interstitial water chemistry at this site is controlled dominantly by the high carbonate and low organic carbon concentrations in the sediment, which results in extremely modest variations in chemical gradients of many dissolved species. The

chemical gradients found at Site 1086 are even more gradual than those found at Site 1085.

### Alkalinity, Sulfate, and Ammonium

Downcore profiles of alkalinity, sulfate, and ammonium (Fig. 16) reflect the degradation of the low concentrations of organic matter. Alkalinity reaches a maximum value of only 17 mM at 125 mbsf and subsequently decreases to the bottom of the hole. Compared with other Leg 175 sites, this is an extremely deep stratigraphic position for the alkalinity maximum, with most alkalinity maxima at the previous sites being reached within the uppermost 50 to 100 mbsf. Sulfate is consumed by 180 mbsf, which is also very deep in comparison with the previous Leg 175 sites. This very weak gradient reflects both the low level of organic carbon (see "Organic Geochemistry" section, this chapter) as well as the low sedimentation rate (see "Biostratigraphy and Sedimentation Rates" section, this chapter). Ammonium reaches a maximum of only ~2800 μM at 125 mbsf. As with the alkalinity profile at this site, this concentration is very low compared with other Leg 175 sites and reflects the small amount of organic matter.

### Calcium, Magnesium, and Strontium

The concentration of dissolved Sr<sup>2+</sup> increases essentially linearly to a maximum value of 312 μM at the bottom of the hole (Fig. 17).

The overall increase downhole records the dissolution of biogenic calcite, which releases Sr<sup>2+</sup> to the interstitial waters. The rate of increase of dissolved Sr<sup>2+</sup> is strongly similar to that observed at Site 1085, reflecting the common influence of the high concentrations of biogenic calcium carbonate in the sediment from these two sites (see "Organic Geochemistry" section, this chapter).

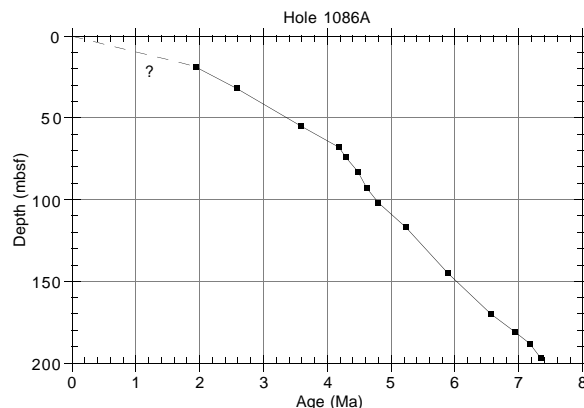


Figure 12. Relation between depth below seafloor and age at Hole 1086A, based on the magnetostratigraphic interpretation in Table 6.

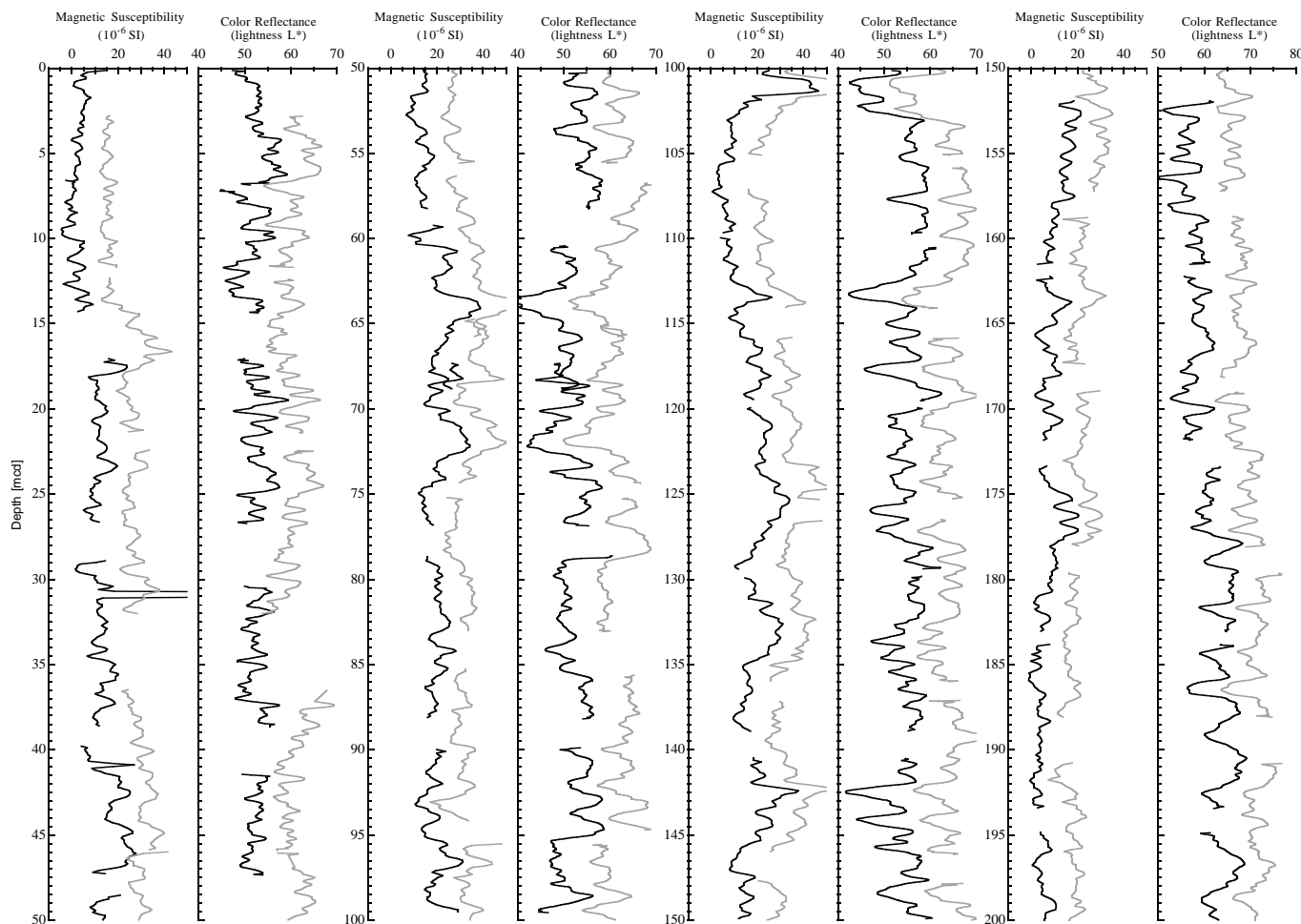


Figure 13. Composite section for Site 1086. Magnetic susceptibility and color reflectance (lightness L\*) data are plotted for Holes 1086 A (black line) and 1086B (gray line). Note the scale shift for the rightmost plot of lightness (L\*). The downhole logs are shown in meters composite depth (mcd). An offset of 1.5 times the standard deviation of Hole 1086A data have been added to Hole 1086B for clarity in viewing the composite section. (Continued next page.)

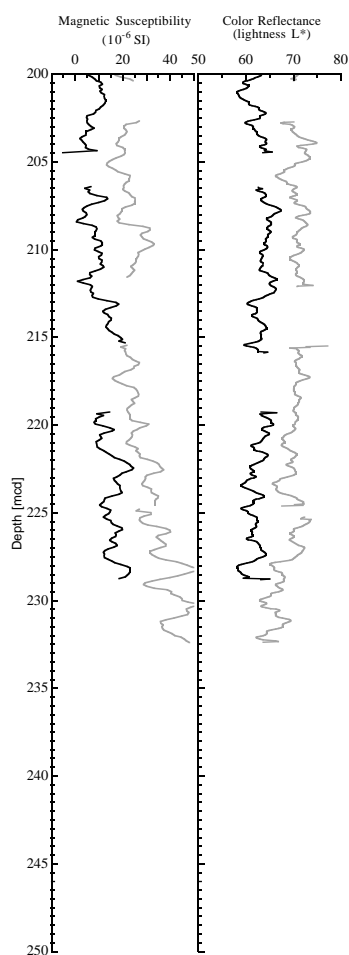


Figure 13 (continued).

Dissolved  $\text{Ca}^{2+}$  decreases by only 5 mM from the seafloor to 96.6 mbsf (Fig. 17). Compared with the decrease observed at Site 1085, this decrease is very gradual. Below 96.6 mbsf, dissolved  $\text{Ca}^{2+}$  remains essentially constant at ~6.5 mM. Dissolved  $\text{Mg}^{2+}$  decreases continually from the seafloor to total depth, with a low value of 30.5 mM. Through the interval in which  $\text{Ca}^{2+}$  decreases by 5 mM,  $\text{Mg}^{2+}$  decreases by 12 mM. This lack of correspondence in both extent and pattern of the respective decreases suggests that dolomitization is less important than at other Leg 175 sites. Rather, we attribute the decrease in  $\text{Ca}^{2+}$  to phosphate precipitation and the decrease in  $\text{Mg}^{2+}$  to clay mineral uptake, with only a minor effect from dolomitization.

### Silica and Phosphate

Dissolved silica is present in interstitial waters from Site 1086 at concentrations greater than representative bottom-water values (Fig. 18), indicating dissolution of biogenic opal. The rapid increase through the uppermost 30 mbsf is also consistent with the fact that siliceous sponge spicules are abundant and serve as a source of dissolved silica. Although the concentration of dissolved silica is relatively low throughout the entire sequence in the absolute sense, a maximum of ~600  $\mu\text{M}$  is found at 30 mbsf with a rapid decrease of values below that depth. This pattern of dissolved silica is consistent with the lack of siliceous microfossils below 35 mbsf, and thus a source of dissolved silica is missing from this deeper portion of the sequence.

Dissolved phosphate concentrations increase only very slightly with depth and reach a maximum of only 21  $\mu\text{M}$  at 49 mbsf (Fig. 18). The maximum itself is very broad and diffuse. Toward the deeper portion of the sequence, dissolved phosphate concentrations decrease

Table 7. Offsets applied to cores from Holes 1086A and 1086B.

Core	Depth (mbsf)	Offset (m)	Composite depth (mcd)
175-1086A-			
1H	0.0	0.10	0.10
2H	16.2	-0.16	16.04
3H	25.7	0.80	26.50
4H	35.2	3.16	38.36
5H	44.7	4.54	49.24
6H	54.2	3.80	58.00
7H	63.7	4.98	68.68
8H	73.2	3.58	76.78
9H	82.7	5.37	88.07
10H	92.2	7.15	99.35
11H	101.7	7.91	109.61
12H	111.2	8.11	119.31
13H	120.7	8.67	129.37
14H	130.2	9.07	139.27
15H	139.7	10.27	149.97
16H	149.2	12.17	161.37
17H	158.7	12.99	171.69
18H	168.2	14.61	182.81
19H	177.7	15.57	193.27
20H	187.2	17.13	204.33
21H	196.7	19.17	215.87
175-1086B-			
1H	0.3	-0.10	0.20
2H	9.8	2.44	12.24
3H	19.3	2.50	21.80
4H	28.8	3.06	31.86
5H	38.3	7.64	45.94
6H	47.8	7.64	55.44
7H	57.3	8.50	65.80
8H	66.8	7.40	74.20
9H	76.3	8.36	84.66
10H	85.8	8.93	94.73
11H	95.3	9.67	104.97
12H	104.8	10.31	115.11
13H	114.3	10.97	125.27
14H	123.8	12.11	135.91
15H	133.3	13.23	146.53
16H	142.8	14.35	157.15
17H	152.3	15.83	168.13
18H	161.8	16.59	178.39
19H	171.3	17.75	189.05
20H	180.8	19.43	200.23
21H	190.3	21.83	212.13
22H	199.8	25.11	224.91

Note: The offsets transform ODP standard depth values in meters below seafloor (mbsf) to meters composite depth (mcd).

to values <10  $\mu\text{M}$ , most likely reflecting authigenic phosphate precipitation.

### Sodium and Potassium

Dissolved  $\text{Na}^+$  increases rapidly through the uppermost 30 mbsf and is relatively constant to the bottom of the hole (Fig. 19). Concentrations of dissolved  $\text{K}^+$  are relatively constant through the uppermost 68 mbsf and then decrease to the bottom of the hole. The concentrations of both of these cations are lower at Site 1086 than at Site 1085.

### Salinity and Chloride

Salinity decreases slightly through the sequence (Fig. 20), recording the total decreases in the dissolved species described above, particularly alkalinity,  $\text{Mg}^{2+}$ , and  $\text{K}^+$ . Concentrations of dissolved  $\text{Cl}^-$  record an initial increase to a maximum of ~557 mM (30–40 mbsf) before decreasing to the bottom of the hole. This initial increase in dissolved  $\text{Cl}^-$  may reflect changes in bottom-water chemistry associated with ice-volume variations through glacial periods. Both the salinity and  $\text{Cl}^-$  profiles are very similar to those observed at Site 1085.

### ORGANIC GEOCHEMISTRY

Calcium carbonate and organic carbon concentrations were measured on sediment samples from Hole 1086A (Table 10). Organic matter atomic carbon/nitrogen (C/N) ratios were employed to identify

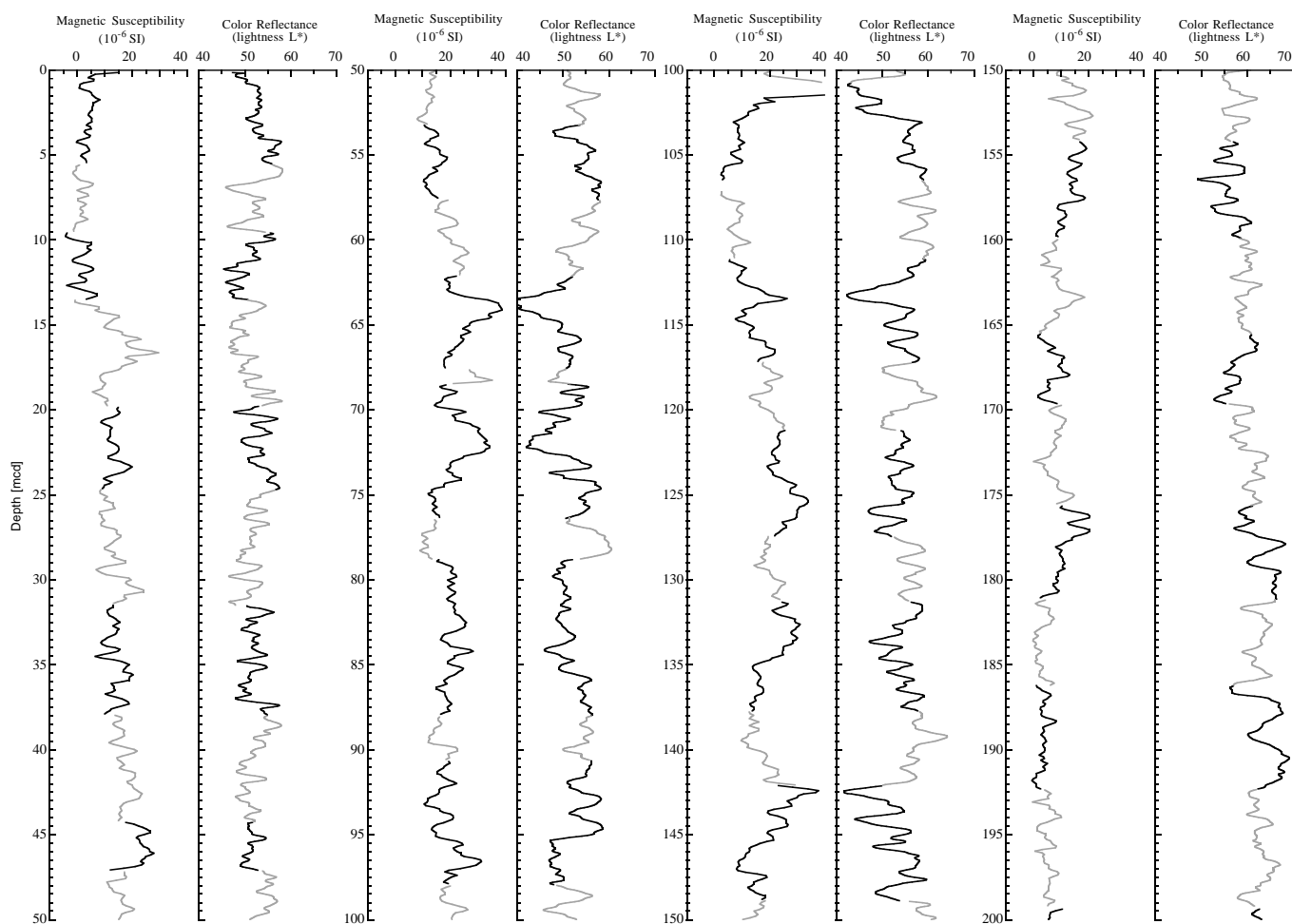


Figure 14. Spliced records for magnetic susceptibility and color reflectance (lightness  $L^*$ ) plotted in meters composite depth (mcd). Cores from two holes at Site 1086 have been used for the spliced record: black line = Hole 1086A and gray line = Hole 1086B. (Continued next page.)

the origin of organic matter contained within the sediments. Moderate amounts of gas were encountered, and routine monitoring of the sedimentary gases was done for drilling safety.

### Inorganic and Organic Carbon Concentrations

Concentrations of carbonate carbon in Site 1086 sediments range between 10.6 and 7.6 wt%, corresponding to 88.7 and 63.0 wt%  $\text{CaCO}_3$  (Table 10). Despite considerable fluctuations in carbonate concentrations (Fig. 21), the sediments at this site represent a single lithostratigraphic unit (see “Lithostratigraphy” section, this chapter). This unit averages 79 wt%  $\text{CaCO}_3$ .

TOC determinations were done on selected samples of Hole 1086A sediments to estimate the amounts of organic matter in the sediments (Table 10). TOC concentrations vary between 3.56 wt% and values below detection ( $<0.05$  wt%) and generally decrease with sediment depth (Fig. 22). Their average value is 1.11 wt%. These TOC concentrations reflect a history of moderate-to-low productivity in this part of the Benguela Current system, which has delivered only modest amounts of organic matter to the sediments, and the low accumulation rate of sediments (see “Biostratigraphy and Sedimentation Rates” section, this chapter), which is detrimental to preservation of organic matter.

### Organic Matter Source Characterization

Organic C/N ratios were calculated for sediment samples using TOC and total nitrogen concentrations (Table 10). For those samples having nitrogen concentrations below the limit of reliable measurement (0.05 wt%), C/N values have been excluded. The C/N ratios vary from 13.9 to 4.3 (Fig. 23) and average 8.6. Many of these C/N ratios are intermediate between unaltered algal organic matter (5–8) and fresh land-plant material (25–35; e.g., Emerson and Hedges, 1988; Meyers, 1994). Because of their setting seaward of a major upwelling system and offshore from a coastal desert, however, it is likely that these sediments contain mostly marine-derived organic matter with only a minor contribution of detrital continental organic matter.

### Headspace Gases

Low amounts of methane ( $\text{C}_1$ ) and  $\text{CO}_2$  were found in sediments from Site 1086. Methane first appears in headspace gas samples from Hole 1086A sediments at 6 mbsf, but concentrations never become significant (Table 11). The origin of the methane is probably from in situ microbial fermentation of the marine organic matter present in the sediments, and the low availability of organic matter limits gas production. A biogenic origin of the methane is supported by the dis-

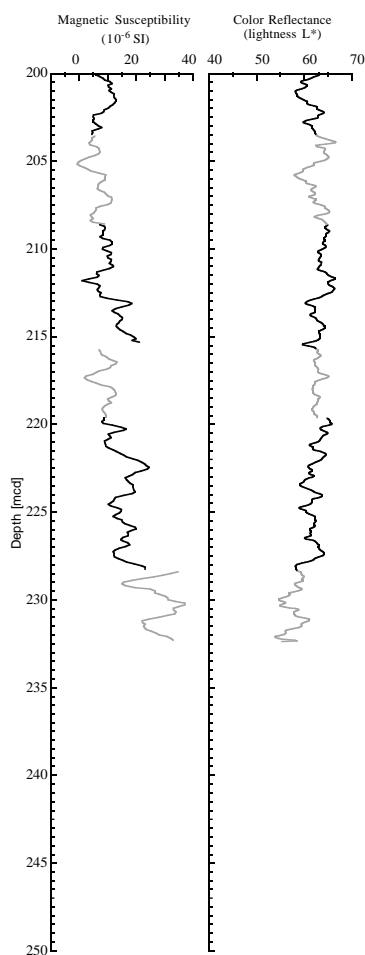


Figure 14 (continued).

appearance of interstitial sulfate at approximately the same sub-bottom depth where methane concentrations begin to rise (see “Inorganic Geochemistry” section, this chapter), inasmuch as Claypool and Kvenvolden (1983) observe that the presence of interstitial sulfate inhibits microbial methanogenesis in marine sediments.

The most abundant gas was  $\text{CO}_2$ , and headspace concentrations of this gas remained high deep in Hole 1086A (201 mbsf; Table 11). Cragg et al. (1992) isolated viable microbes to depths of ~500 mbsf in sediments from the Japan Sea. The presence of small amounts of biogenic gases in sediments from Site 1086 suggests the presence of similarly viable microbial communities throughout the sedimentary sequence at this location, but their activity has been limited by the low availability of organic matter.

## PHYSICAL PROPERTIES

A minimum program of shipboard physical properties measurements was carried out at Site 1086. Measurements with the MST were conducted at a low resolution on GRAPE wet bulk density, magnetic susceptibility, and  $P$ -wave velocity on all recovered whole-round core sections.

Gravimetric wet bulk density, porosity, and moisture content data were determined from one sample point in every half-split core section. Method C was used at Site 1086 (see “Explanatory Notes” chap-

ter, this volume). Undrained vane shear strength was not measured because of time constraints at this alternate site.

Discrete compressional ( $P$ -wave) velocity measurements were made at a resolution of one sampling point per section. For these  $P$ -wave velocity measurements, the modified Hamilton Frame was used on split sections of cores between 0 and 207 mbsf.

Thermal conductivity was determined on every fifth unsplit section in every core by inserting a thermal probe into the sediment (see “Explanatory Notes” chapter, this volume).

## Multisensor Track

GRAPE density (Fig. 24),  $P$ -wave velocity (Fig. 25), and magnetic susceptibility (Fig. 26A) were recorded every 10 cm for the entire depth at Hole 1086A. MST data are included on CD-ROM (back pocket, this volume). Compressional velocities were stored at an amplitude threshold of 50 incremental units. The MST  $P$ -wave logger recorded signals over the entire depth of 207 mbsf at Hole 1086A (Fig. 25). This long MST  $P$ -wave profile indicates a low gas content and low signal attenuation in the sediments. MST velocity and discrete velocities correlate well over the entire depth range, although discrete velocities were mostly higher (Fig. 25).

Magnetic susceptibility (Fig. 26A) shows a similar trend compared with GRAPE and index properties wet bulk density (Figs. 24, 27A).

GRAPE density and index properties wet bulk density display a high degree of similarity. GRAPE density shows an overall increase from 1530 to 1950  $\text{kg/m}^3$  because of sediment compaction. Long-term variations in GRAPE density may correspond to lithologic boundaries (see “Lithostratigraphy” section, this chapter). Unlike at other Leg 175 sites, higher values in GRAPE density than in the wet bulk density can be observed over the entire depth range at Site 1086.

## Velocities

Between 0 and 207 mbsf, most of the MST  $P$ -wave values are lower than the discrete velocities (Fig. 25). Because of the much lower gas content observed at Hole 1086A (see “Organic Geochemistry” section, this chapter), the recovered sediments were much less disturbed. Thus, velocity data from Hole 1086A are of better quality than velocity data from previous Leg 175 sites, where higher gas content caused numerous voids and cracks. Discrete velocities reveal high values in the top portion of Hole 1086A (Fig. 25), which may be caused by coarser grained particles (see “Lithostratigraphy” section, this chapter).

## Index Properties

Data from discrete measurements of wet bulk density, porosity, and moisture content are displayed in Figures 27A, 27B, and 27C, respectively (also see Table 12 on CD-ROM, back pocket, this volume). The density values vary between 1500 and 1870  $\text{kg/m}^3$ , indicating a coarser grain-size distribution in the sediments compared with previous Leg 175 sites.

The wet bulk density profile shows an overall increase, which can be mostly assigned to compaction. Hole 1086A consists mainly of foraminifer-nannofossil ooze (see “Lithostratigraphy” section, this chapter). This sediment composition is reflected in higher velocities (Fig. 25), although maximum values in the velocity profile do not necessarily correspond to maximum wet bulk density values (Fig. 24).

In general, porosity and moisture profiles are inversely correlated with the wet bulk density. Porosities decrease from 70% in the top section to 52% at 207 mbsf (Fig. 27B). Moisture content varies between 48% at the top of Hole 1086A and 28% at 207 mbsf (Fig. 27C).

**Table 8. List of splice tie points used to create the continuous “spliced” stratigraphic sequence for Site 1086.**

Hole, core, section, interval (cm)	Depth (mbsf)	Composite depth (mcd)	Whether tied	Hole, core, section, interval (cm)	Depth (mbsf)	Composite depth (mcd)	Offset (m)
1086A-1H-4, 92	5.42	5.52	Tie to	1086B-2H-2, 128	3.08	5.52	2.44
1086B-2H-5, 80	7.10	9.54	Tie to	1086A-2H-2, 150	9.70	9.54	-0.16
1086A-2H-5, 96	13.66	13.50	Tie to	1086B-3H-1, 120	11.00	13.50	2.50
1086B-3H-5, 144	17.24	19.74	Tie to	1086A-3H-2, 124	18.94	19.74	0.80
1086A-3H-6, 20	23.90	24.70	Tie to	1086B-4H-2, 84	21.64	24.70	3.06
1086B-4H-7, 12	28.42	31.48	Tie to	1086A-4H-2, 112	28.32	31.48	3.16
1086A-4H-7, 12	34.82	37.98	Tie to	1086B-5H-2, 4	30.34	37.98	7.64
1086B-5H-6, 28	36.58	44.22	Tie to	1086A-5H-3, 148	39.68	44.22	4.54
1086A-5H-5, 136	42.56	47.10	Tie to	1086B-6H-1, 116	39.46	47.10	7.64
1086B-6H-5, 128	45.58	53.22	Tie to	1086A-6H-4, 21	49.42	53.22	3.80
1086A-6H-7, 12	53.82	57.62	Tie to	1086B-7H-1, 132	49.12	57.62	8.50
1086B-7H-4, 132	53.62	62.12	Tie to	1086A-7H-2, 144	57.14	62.12	4.98
1086A-7H-6, 88	62.58	67.56	Tie to	1086B-8H-2, 136	60.16	67.56	7.40
1086B-8H-3, 76	61.06	68.46	Tie to	1086A-8H-1, 117	64.88	68.46	3.58
1086A-8H-7, 20	72.80	76.38	Tie to	1086B-9H-2, 14.5	68.02	76.38	8.36
1086B-9H-3, 104	70.41	78.77	Tie to	1086A-9H-1, 20	73.40	78.77	5.37
1086A-9H-7, 52	82.62	87.99	Tie to	1086B-10H-2, 125	79.06	87.99	8.93
1086B-10H-4, 88	81.68	90.61	Tie to	1086A-10H-1, 76	83.46	90.61	7.15
1086A-10H-6, 68	90.78	97.93	Tie to	1086B-11H-2, 96	88.26	97.93	9.67
1086B-11H-4, 76	91.06	100.73	Tie to	1086A-11H-1, 62	92.82	100.73	7.91
1086A-11H-5, 36	98.56	106.47	Tie to	1086B-12H-1, 85	96.16	106.47	10.31
1086B-12H-4, 96	100.76	111.07	Tie to	1086A-12H-1, 125	102.96	111.07	8.11
1086A-12H-5, 140	109.10	117.21	Tie to	1086B-13H-1, 144	106.24	117.21	10.97
1086B-13H-4, 92	110.27	121.19	Tie to	1086A-13H-1, 132	112.52	121.19	8.67
1086A-13H-6, 8	118.78	127.45	Tie to	1086B-14H-1, 104	115.34	127.45	12.11
1086B-14H-4, 32	119.12	131.23	Tie to	1086A-14H-1, 146	122.16	131.23	9.07
1086A-14H-6, 44	128.64	137.71	Tie to	1086B-15H-1, 68	124.48	137.71	13.23
1086B-15H-4, 56	128.86	142.09	Tie to	1086A-15H-2, 12	131.82	142.09	10.27
1086A-15H-6, 92	138.62	148.89	Tie to	1086B-16H-1, 124	134.54	148.89	14.35
1086B-16H-5, 52	139.82	154.17	Tie to	1086A-16H-2, 80	142.00	154.17	12.17
1086A-16H-6, 52	147.72	159.89	Tie to	1086B-17H-1, 125	144.06	159.89	15.83
1086B-17H-5, 88	149.68	165.51	Tie to	1086A-17H-3, 32	152.52	165.51	12.99
1086A-17H-5, 144	156.64	169.63	Tie to	1086B-18H-1, 73	153.04	169.63	16.59
1086B-18H-5, 72	159.02	175.61	Tie to	1086A-18H-2, 80	161.00	175.61	14.61
1086A-18H-6, 32	166.52	181.13	Tie to	1086B-19H-2, 8	163.38	181.13	17.75
1086B-19H-5, 64	168.44	186.19	Tie to	1086A-19H-2, 90	170.62	186.19	15.57
1086A-19H-6, 104	176.74	192.31	Tie to	1086B-20H-2, 8	172.88	192.31	19.43
1086B-20H-6, 96	179.76	199.19	Tie to	1086A-20H-3, 136	182.06	199.19	17.13
1086A-20H-6, 116	186.36	203.49	Tie to	1086B-21H-1, 85	181.66	203.49	21.83
1086B-21H-4, 148	186.78	208.61	Tie to	1086A-21H-2, 73	189.44	208.61	19.17
1086A-21H-7, 32	196.52	215.69	Tie to	1086B-22H-1, 28	190.58	215.69	25.11
1086B-22H-3, 120	194.50	219.61	Tie to	1086A-22H-1, 40	197.10	219.61	22.51
1086A-22H-7, 12	205.82	228.33	Tie to	1086B-23H-3, 57	203.38	228.33	24.95
1086B-23H-6, 12	207.42	232.37					

Note: The tie points are listed in standard ODP meters below seafloor (mbsf) and meters composite depth (mcd).

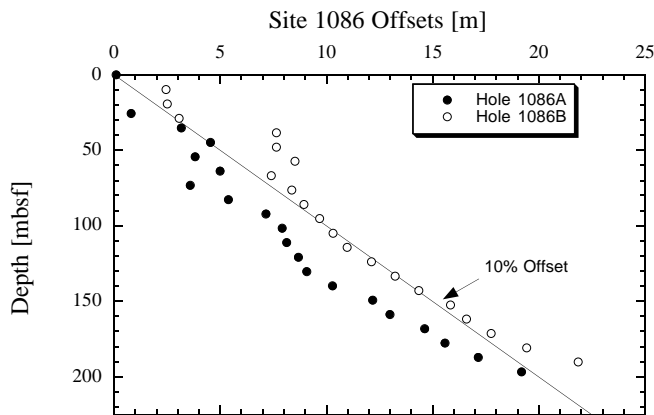


Figure 15. Core offsets applied to Site 1086 plotted against standard ODP mbsf. A linear 10% growth of meters composite depth (mcd) compared with meters below seafloor (mbsf) is indicated by a line.

### Thermal Conductivity

The thermal conductivity profile (Fig. 26B at Hole 1086A was measured in every second and fifth core section above 40 mbsf and in every fifth section below 40 mbsf (see “Explanatory Notes” chap-

ter, this volume). Values range between 0.8 and 1.32 W/(m·K) and are higher than at any other Leg 175 site. Despite the low resolution sampling, a good match among thermal conductivity, magnetic susceptibility, and GRAPE density can be observed (Fig. 24; also see Table 12 on CD-ROM, back pocket, this volume). Elevated values in thermal conductivity appear to be related to sediments composed of coarser grained particles such as quartz minerals (see “Lithostratigraphy” section, this chapter).

### REFERENCES

Austin, J.A., Jr., and Uchupi, E., 1982. Continental-oceanic crustal transition off Southwest Africa. *AAPG Bull.*, 66:1328–1347.

Berger, W.H., Burke, S., and Vincent, E., 1987. Glacial-Holocene transition: climate pulsations and sporadic shutdown of NADW production. In Berger, W.H., and Labeyrie, L.D. (Eds.), *Abrupt Climatic Change: Evidence and Implications*: Dordrecht (Reidel), 279–297.

Berger, W.H., Killingley, J.S., Metzler, C.V., and Vincent, E., 1985. Two-step deglaciation: <sup>14</sup>C-dated high-resolution <sup>18</sup>O records from the tropical Atlantic Ocean. *Quat. Res.*, 23:258–271.

Berggren, W.A., Kent, D.V., Swisher, C.C., III, and Aubry, M.-P., 1995. A revised Cenozoic geochronology and chronostratigraphy. In Berggren, W.A., Kent, D.V., Aubry, M.-P., and Hardenbol, J. (Eds.), *Geochronology, Time Scales and Global Stratigraphic Correlation*. Spec. Publ.—Soc. Econ. Paleontol. Mineral. (Soc. Sediment. Geol.), 54:129–212.

Bleil, U., and Shipboard Scientific Party, 1996. Report and preliminary results of METEOR cruise M34/1, Capetown-Walvis Bay, 3.1.1996–26.1.1996. *Ber. Fachber. Geowiss., Univ. Bremen*, 77.

- Blow, W.H., 1969. Late middle Eocene to Recent planktonic foraminiferal biostratigraphy. In Brönnimann, P., and Renz, H.H. (Eds.), *Proc. First Int. Conf. Planktonic Microfossils, Geneva, 1967*: Leiden (E.J. Brill), 1:199–422.
- Boersma, A., 1984. *A Handbook of Common Tertiary Uvigerina*: Stony Point, NY (Microclimates Press).
- Bolli, H.M., Ryan, W.B.F., et al., 1978. *Init. Repts. DSDP*, 40: Washington (U.S. Govt. Printing Office).
- Bolli, H.M., and Saunders, J.B., 1985. Oligocene to Holocene low latitude planktic foraminifera. In Bolli, H.M., Saunders, J.B., and Perch-Nielsen, K. (Eds.), *Plankton Stratigraphy*: Cambridge (Cambridge Univ. Press), 155–262.
- Claypool, G.E., and Kvenvolden, K.A., 1983. Methane and other hydrocarbon gases in marine sediment. *Annu. Rev. Earth Planet. Sci.*, 11:299–327.
- Cragg, B.A., Harvey, S.M., Fry, J.C., Herbert, R.A., and Parkes, R.J., 1992. Bacterial biomass and activity in the deep sediment layers of the Japan Sea, Hole 798B. In Pisciotto, K.A., Ingle, J.C., Jr., von Breyman, M.T., Barron, J., et al., *Proc. ODP, Sci. Results.*, 127/128 (Pt. 1): College Station, TX (Ocean Drilling Program), 761–776.
- Dingle, R.V., 1980. Large allocthonous sediment masses and their role in the construction of the continental slope and rise off Southwestern Africa. *Mar. Geol.*, 37:333–354.
- Dingle, R.V., Birch, G.F., Bremner, J.M., de Decker, R.H., du Plessis, A., Engelbrecht, J.C., Finchan, M.J., Fitton, T., Flemming, B.W., Gentle, R.L., Goodlad, S.W., Martin, A.K., Mills, E.G., Moir, G.J., Parker, R.J., Robson, S.H., Rogers, J., Salmon, D.A., Siesser, W.G., Simpson, E.S.W., Summerhayes, C.P., Westall, C.F., and Winter, A., 1987. Deep-sea sedimentary environments around southern Africa, South-East Atlantic and South-West Indian Oceans. *Ann. S. Afr. Mus.*, 98:1–27.
- Dingle, R.V., and Robson, S.H., 1992. Southwestern Africa continental rise: structural and sedimentary evolution. In Poag, C.W., and Graciansky, P.C. (Eds.), *Geologic Evolution of Atlantic Continental Rises*: New York (Van Nostrand), 62–76.
- Emerson, S., and Hedges, J.I., 1988. Processes controlling the organic carbon content of open ocean sediments. *Paleoceanography*, 3:621–634.
- Emery, K.O., Uchupi, E., Bowin, C.O., Phillips, J., and Simpson, E.S.W., 1975. Continental margin off western Africa: Cape St. Francis (South Africa) to Walvis Ridge (South-West Africa). *AAPG Bull.*, 59:3–59.
- Gerrard, I., and Smith, G.C., 1982. Post-Paleozoic succession and structures of the southwestern African continental margin. In Watkins, J.S., and Drake, C.L. (Eds.), *Studies in Continental Margin Geology*. AAPG Mem., 34:49–74.
- Gordon, A.L., 1986. Inter-ocean exchange of thermocline water. *J. Geophys. Res.*, 91:5037–5046.
- Kennett, J.P., and Srinivasan, M.S., 1983. *Neogene Planktonic Foraminifera: A Phylogenetic Atlas*: Stroudsburg, PA (Hutchinson Ross).
- Lourens, L.J., Antonarakou, A., Hilgen, F.J., Van Hoof, A.A.M., Vergnaud-Grazzini, C., and Zachariasse, W.J., 1996. Evaluation of the Plio-Pleistocene astronomical timescale. *Paleoceanography*, 11:391–413.
- Lutjeharms, J.R.E., 1996. The exchange of water between the South Indian and South Atlantic Ocean. In Wefer, G., Berger, W.H., Siedler, G., and Webb, D.J. (Eds.), *The South Atlantic: Present and Past Circulation*: Berlin (Springer-Verlag), 125–162.
- Martini, E., 1971. Standard Tertiary and Quaternary calcareous nannoplankton zonation. In Farinacci, A. (Ed.), *Proc. 2nd Int. Conf. Planktonic Microfossils Roma*: Rome (Ed. Tecnosci.), 2:739–785.
- McIntyre, A., Ruddiman, W.F., Karlin, K., and Mix, A.C., 1989. Surface water response of the equatorial Atlantic Ocean to orbital forcing. *Paleoceanography*, 4:19–55.
- Meyers, P.A., 1994. Preservation of elemental and isotopic source identification of sedimentary organic matter. *Chem. Geol.*, 144:289–302.
- Millero, F.J., and Sohn, M.L., 1992. *Chemical Oceanography*: Boca Raton (CRC Press).
- Okada, H., and Bukry, D., 1980. Supplementary modification and introduction of code numbers to the low-latitude coccolith biostratigraphic zonation (Bukry, 1973; 1975). *Mar. Micropaleontol.*, 5:321–325.
- Rintoul, S.R., 1991. South Atlantic interbasin exchange. *J. Geophys. Res.*, 96:2675–2692.
- Wefer, G., Berger, W.H., Bickert, T., Donner, B., Fischer, G., Kemle-von Mücke, S., Meinecke, G., Müller, P.J., Multiza, S., Niebler, H.-S., Pätzold, J., Schmidt, H., Schneider, R.R., and Segl, M., 1996. Late Quaternary surface circulation of the South Atlantic: the stable isotope record and implications for heat transport and productivity. In Wefer, G., Berger, W.H., Siedler, G., and Webb, D.J. (Eds.), *The South Atlantic: Present and Past Circulation*: Berlin (Springer-Verlag), 461–502.

Ms 175IR-114

**NOTE: Core-description forms (“barrel sheets”) and core photographs can be found in Section 4, beginning on page 581. Forms containing smear-slide data can be found on CD-ROM. See Table of Contents for materials contained on CD-ROM.**

Table 9. Interstitial water composition for Hole 1086A.

Core, section, interval (cm)	Depth (mbsf)	pH	Alkalinity (mM)	Salinity	Cl <sup>-</sup> (titr) (mM)	Cl <sup>-</sup> (IC) (mM)	SO <sub>4</sub> <sup>2-</sup> (mM)	Na <sup>+</sup> (mM)	Mg <sup>2+</sup> (mM)	Ca <sup>2+</sup> (mM)	K <sup>+</sup> (mM)	H <sub>4</sub> SiO <sub>4</sub> (μM)	NH <sub>4</sub> <sup>+</sup> (μM)	PO <sub>4</sub> <sup>3-</sup> (μM)	Sr <sup>2+</sup> (μM)
175-1086A-															
1H-1, 140-150	1.40	7.57	2.922	35.0	544	539	27.35	464	52.40	11.09	10.61	116	181	5	94
1H-3, 140-150	4.40	7.10	3.547	35.0	550	538	26.54	472	51.83	10.06	10.73	259	403	8	96
2H-3, 140-150	11.10	6.64	4.883	35.0	552	544	25.31	475	51.13	9.45	10.77	409	904	10	106
3H-3, 140-150	20.60	7.63	8.027	35.0	553	579	23.93	477	50.71	9.58	10.97	545	1117	12	117
4H-3, 140-150	30.10	7.67	8.833	35.0	557	558	20.83	481	48.96	8.87	10.56	571	1746	11	123
5H-3, 140-150	39.60	7.70	10.324	34.5	555	551	18.43	479	47.97	8.58	10.54	502	1644	14	134
6H-3, 140-150	49.10	7.76	11.716	34.0	554	549	15.28	476	46.90	7.92	10.27	395	1661	21	140
7H-3, 140-150	58.60	7.77	12.559	34.0	552	547	13.24	474	45.84	7.74	10.23	326	1882	17	154
8H-3, 130-140	68.00	7.78	13.829	33.5	552	546	11.74	477	43.81	7.25	10.17	304	2086	16	169
9H-3, 130-140	77.50	7.79	14.456	33.5	552	550	10.23	481	41.87	6.47	9.50	295	2146	16	183
10H-3, 130-140	87.00	7.75	14.828	33.5	551	573	9.16	480	41.02	6.14	9.49	316	2018	17	187
11H-3, 140-150	96.60	7.76	15.139	33.0	551	568	6.58	476	40.25	6.56	9.30	352	2367	16	198
14H-3, 140-150	125.10	7.72	17.356	32.5	548	569	3.91	478	36.73	6.46	8.67	419	2809	9	227
17H-3, 140-150	153.60	7.58	16.338	32.0	547	547	1.48	479	33.70	6.13	7.90	381	2698	12	256
20H-3, 140-150	182.10	7.59	15.293	32.0	547	531	0.00	479	31.75	6.32	7.85	400	2613	9	288
22H-3, 140-150	201.10	7.03	14.035	32.0	544	542	0.00	476	30.50	6.48	7.94	404	2477	5	312

Note: Cl<sup>-</sup> (titr) = analyzed by titration and Cl<sup>-</sup> (IC) = analyzed by ion chromatography.

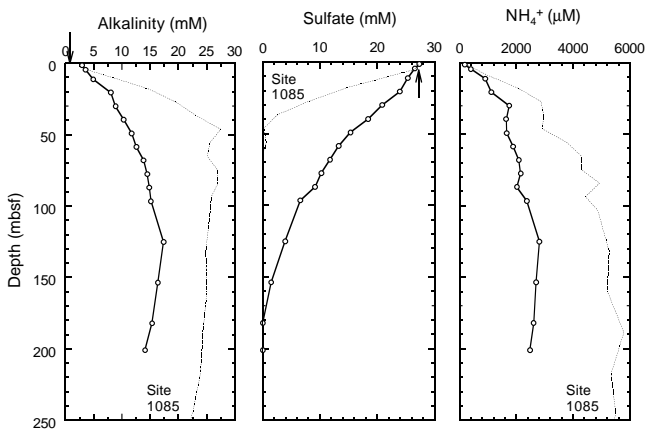


Figure 16. Downcore profiles of dissolved alkalinity, sulfate, and ammonium at Site 1086 (solid lines with open circles). Profile from Site 1085 (dotted lines) is shown for comparison. Arrows = mean ocean-bottom-water values taken from Millero and Sohn (1992).

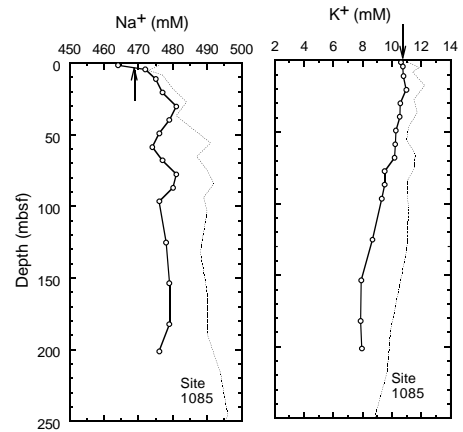


Figure 19. Downcore profiles of dissolved Na<sup>+</sup> and K<sup>+</sup> at Site 1086 (solid lines with open circles). Profile from Site 1085 (dotted lines) is shown for comparison. Arrows = mean ocean-bottom-water values taken from Millero and Sohn (1992).

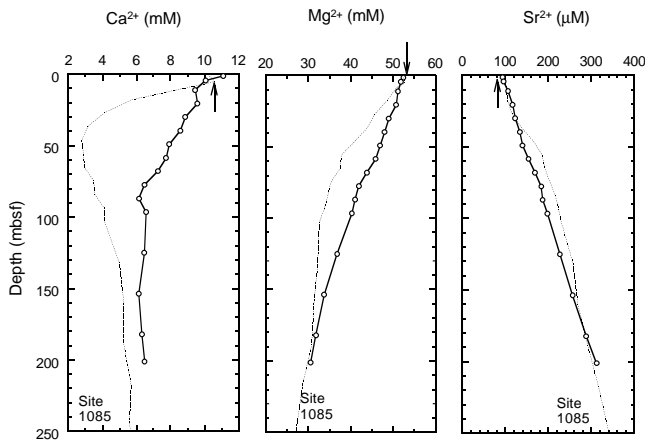


Figure 17. Downcore profiles of Ca<sup>2+</sup>, Mg<sup>2+</sup>, and Sr<sup>2+</sup> at Site 1086 (solid lines with open circles). Profile from Site 1085 (dotted lines) is shown for comparison. Arrows = mean ocean-bottom-water values taken from Millero and Sohn (1992).

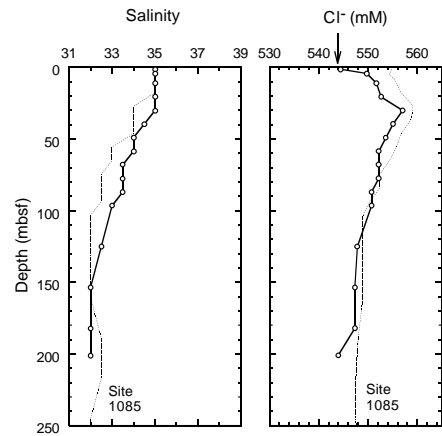


Figure 20. Downcore profiles of salinity and dissolved Cl<sup>-</sup> at Site 1086 (solid lines with open circles). Profile from Site 1085 (dotted lines) is shown for comparison. Arrow = mean ocean-bottom-water value taken from Millero and Sohn (1992).

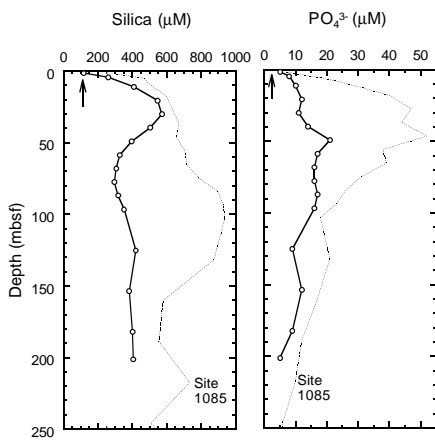


Figure 18. Downcore profiles of dissolved silica and phosphate at Site 1086 (solid lines with open circles). Profile from Site 1085 (dotted lines) is shown for comparison. Arrows = mean ocean-bottom-water values taken from Millero and Sohn (1992).

**Table 10. Percentages of inorganic and total carbon, total organic carbon, total nitrogen, and total sulfur in sediment samples from Hole 1086A.**

Core, section, interval (cm)	Depth (mbsf)	IC (wt%)	CaCO <sub>3</sub> (wt%)	TC (wt%)	TOC (wt%)	TN (wt%)	TS (wt%)	C/N (atomic)
175-1086A-								
1H-2, 46-47	1.96	9.94	82.8	10.77	0.83	0.14	0.01	6.8
1H-4, 46-47	4.96	10.05	83.7					
2H-2, 46-47	8.66	10.07	83.9	11.18	1.11	0.15	0.01	8.9
2H-4, 46-47	11.66	9.19	76.6					
3H-2, 46-47	18.16	9.38	78.2	9.97	0.59	0.12	0.15	5.7
3H-4, 46-47	21.16	9.15	76.3					
3H-6, 46-47	24.16	9.60	80.0	10.32	0.71	0.14	0.08	6.1
4H-2, 46-47	27.66	9.10	75.8					
4H-4, 46-47	30.66	9.00	75.0	9.99	0.98	0.14	0.35	7.9
4H-6, 46-47	33.66	9.17	76.4					
5H-2, 46-47	37.16	8.82	73.5	9.89	1.07	0.15	0.31	8.6
5H-4, 46-47	40.16	7.59	63.3					
6H-2, 46-47	46.66	9.29	77.4	10.29	1.00	0.16	0.40	7.5
6H-4, 46-47	49.66	9.02	75.2					
6H-6, 46-47	52.66	9.27	77.2	10.24	0.97	0.15	0.39	7.7
7H-2, 46-47	56.16	8.98	74.8					
7H-4, 46-47	59.16	7.96	66.3	11.51	3.56	0.30	0.77	13.9
7H-6, 46-47	62.16	9.08	75.6					
8H-2, 46-47	65.66	9.01	75.0	10.58	1.57	0.17	0.49	10.8
8H-4, 46-47	68.66	8.47	70.5					
8H-6, 46-47	71.56	9.62	80.1	11.24	1.62	0.17	0.40	11.0
9H-2, 46-47	75.16	8.95	74.5					
9H-4, 46-47	78.06	9.38	78.1	10.69	1.32	0.16	0.44	9.8
9H-6, 46-47	81.06	9.46	78.8					
10H-2, 46-47	84.66	9.33	77.7	11.35	2.02	0.21	0.40	11.4
10H-4, 46-47	87.56	9.70	80.8					
10H-6, 46-47	90.56	8.25	68.7	9.55	1.30	0.17	0.81	9.1
11H-2, 46-47	94.16	9.13	76.0					
11H-4, 46-47	97.16	9.98	83.1	11.32	1.34	0.16	0.30	10.0
11H-6, 46-47	100.16	9.96	83.0					
12H-2, 46-47	103.66	9.57	79.7	10.53	0.96	0.15	0.38	7.6
12H-4, 46-47	106.66	9.76	81.3					
12H-6, 46-47	109.66	8.72	72.6	10.79	2.07	0.20	0.20	12.4
13H-2, 46-47	113.16	9.09	75.7					
13H-4, 46-47	116.16	8.72	72.6					
13H-6, 46-47	119.16	8.79	73.3	9.57	0.78	0.14	0.47	6.7
14H-2, 46-47	122.66	9.19	76.6					
14H-4, 46-47	125.66	8.65	72.1	10.56	1.91	0.19	0.54	11.8
14H-6, 46-47	128.66	9.47	78.9					
15H-2, 46-47	132.16	7.57	63.0	9.93	2.36	0.21	0.75	13.0
15H-4, 46-47	135.16	9.36	78.0					
15H-6, 46-47	138.16	9.12	76.0	10.53	1.41	0.16	0.77	10.1
16H-2, 46-47	141.66	9.62	80.1					
16H-4, 46-47	144.66	9.28	77.3	10.23	0.95	0.13	0.43	8.7
16H-6, 46-47	147.66	9.54	79.5					
17H-2, 46-47	151.16	9.93	82.7	10.47	0.54	0.12	0.25	5.4
17H-4, 46-47	154.16	9.92	82.6					
17H-6, 46-47	157.16	10.12	84.3	10.61	0.49	0.11	0.25	5.3
18H-2, 46-47	160.66	9.36	78.0					
18H-4, 46-47	163.66	10.12	84.3	10.44	0.32	0.09	0.23	4.3
18H-6, 46-47	166.66	10.42	86.8					
19H-2, 46-47	170.16	10.50	87.5	11.08	0.58	0.10	0.27	6.8
19H-4, 46-47	173.16	10.29	85.7					
19H-6, 46-47	176.16	10.65	88.7	11.25	0.60	0.01		
20H-2, 46-47	179.66	10.38	86.4					
20H-4, 46-47	182.66	9.99	83.2	10.73	0.74	0.11	0.25	8.1
20H-6, 46-47	185.66	9.97	83.1					
21H-2, 46-47	189.16	10.47	87.2	11.11	0.64	0.01	0.00	
21H-4, 46-47	192.16	10.13	84.4					
21H-6, 46-47	195.16	10.12	84.3	10.64	0.52	0.11	0.21	5.5
22H-2, 46-47	198.66	10.08	83.9					
22H-4, 46-47	201.66	9.60	80.0	10.18	0.58	0.01	0.31	
22H-6, 46-47	204.66	9.91	82.5	10.16	0.25	0.01	0.30	

Notes: IC = inorganic carbon; CaCO<sub>3</sub> = calcium carbonate; TC = total carbon; TOC = total organic carbon; TN = total nitrogen; TS = total sulfur; and C/N = carbon/nitrogen ratio. TOC concentrations are calculated from the difference between IC and TC concentrations. C/N ratios are calculated from TOC and TN concentrations and are given as atom/atom ratios.

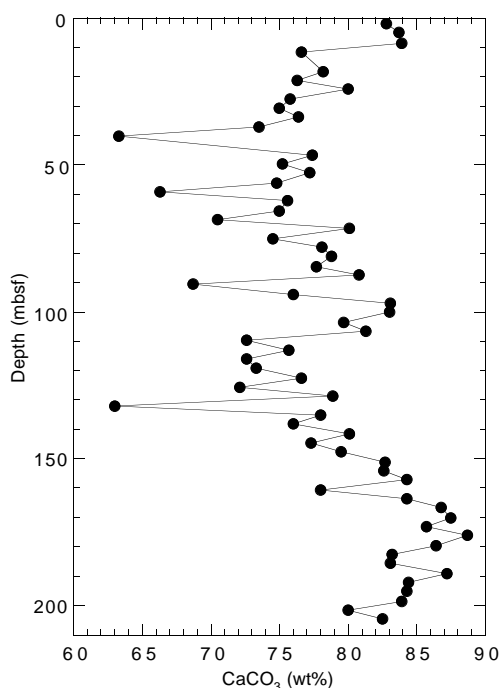


Figure 21. Concentrations of CaCO<sub>3</sub> in sediments from Hole 1086A.

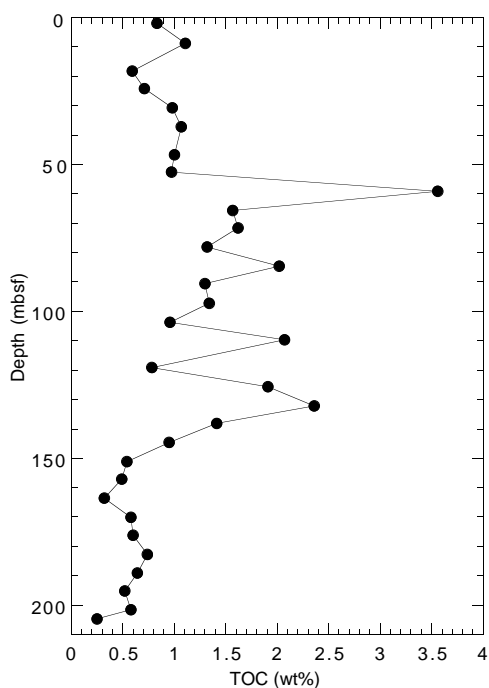


Figure 22. Concentrations of TOC in sediments from Hole 1086A.

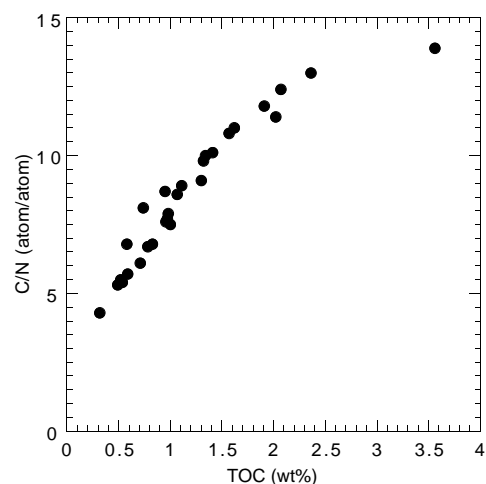


Figure 23. Comparison of organic matter C/N ratios and TOC concentrations of sediments from Hole 1086A. The correspondence between increases in both parameters indicates that preservation of marine organic matter during early diagenesis is important to the TOC contents of sediments on the Namibia margin.

**Table 11. Results of headspace gas analyses of sediments from Hole 1086A.**

Core, section, interval (cm)	Depth (mbsf)	C <sub>1</sub> (ppmv)	CO <sub>2</sub> (ppmv)	C <sub>2</sub> (ppmv)	C <sub>1</sub> /C <sub>2</sub>
175-1086A-					
1H-4, 0-5	4.50	6	5,348		
2H-4, 0-5	11.20	6	4,624		
3H-4, 0-5	20.70	10	7,032		
4H-4, 0-5	30.20	12	8,106	0.2	59
5H-4, 0-5	39.70	15	7,558	0.2	74
6H-4, 0-5	49.20	17	11,755	0.3	57
7H-4, 0-5	58.70	25	14,382	0.6	42
8H-4, 0-5	68.10	26	14,355	0.6	44
9H-4, 0-5	77.60	31	14,779	0.5	62
10H-4, 0-5	87.10	34	15,001	0.5	68
11H-4, 0-5	96.70	37	15,400	0.5	74
12H-7, 0-5	110.70	35	12,886	0.4	87
13H-7, 0-5	120.20	44	14,959	0.6	74
14H-4, 0-5	125.20	42	12,175	0.4	105
15H-7, 0-5	139.20	40	14,681	0.4	100
16H-7, 0-5	148.70	41	11,721	0.3	136
17H-4, 0-5	153.70	58	14,264	0.5	117
18H-7, 0-5	167.70	80	17,337	0.6	133
19H-7, 0-5	177.20	88	19,383	0.6	137
20H-4, 0-5	182.20	101	17,731	0.6	168
21H-7, 0-5	196.20	64	10,655	0.3	214
22H-4, 0-5	201.20	89	16,162	0.4	222

Notes: C<sub>1</sub> = methane; CO<sub>2</sub> = carbon dioxide; and C<sub>2</sub> = ethane. Dominance of C<sub>1</sub> over C<sub>2</sub> indicates that the gases originate from in situ microbial degradation of organic matter.

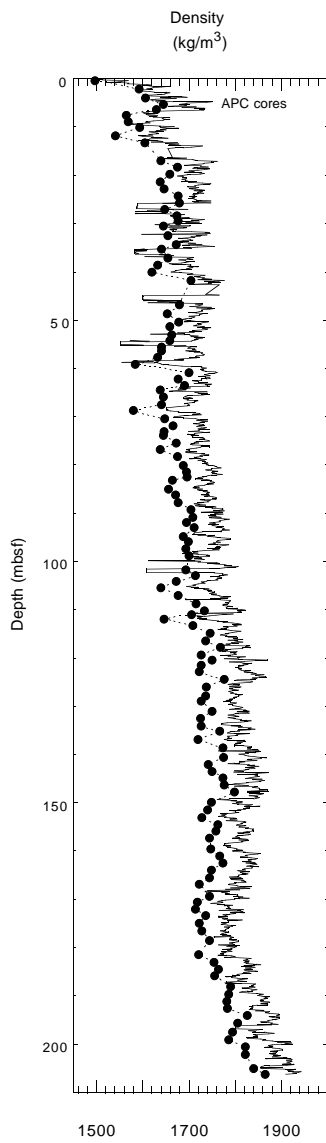


Figure 24. GRAPE wet bulk density data (solid line) compared with index properties gravimetric wet bulk density values (solid circles) for Hole

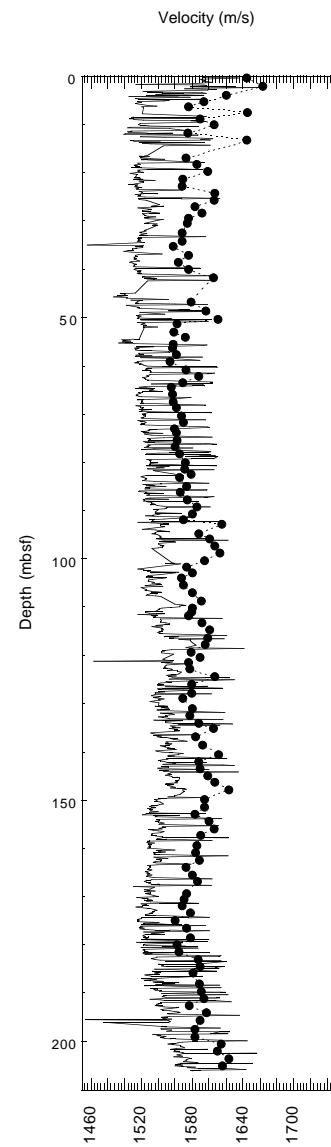


Figure 25. Discrete velocity profile (solid circles) compared with MST velocity data (solid line) measured at Hole 1086A.

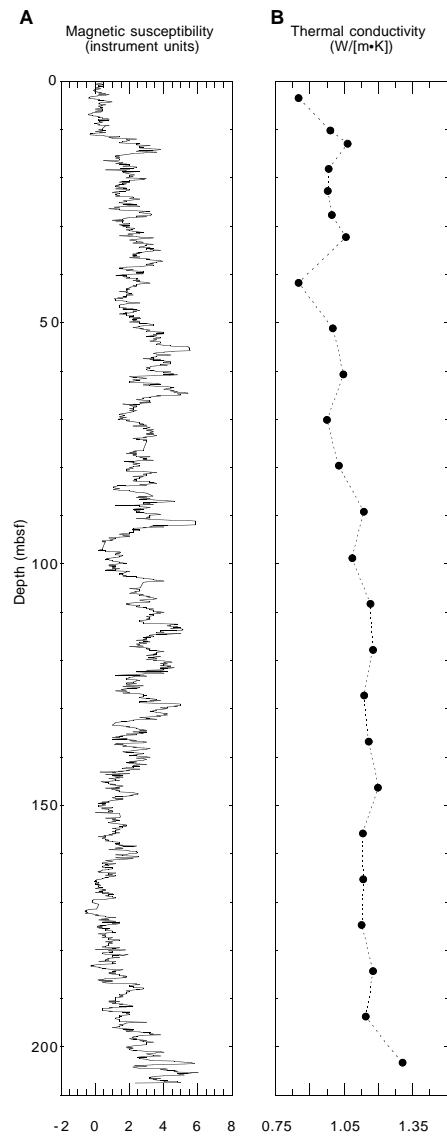


Figure 26. Plots of (A) magnetic susceptibility from MST measurements compared with (B) discrete values of thermal conductivity between 0 and 207 mbsf at Hole 1086A.

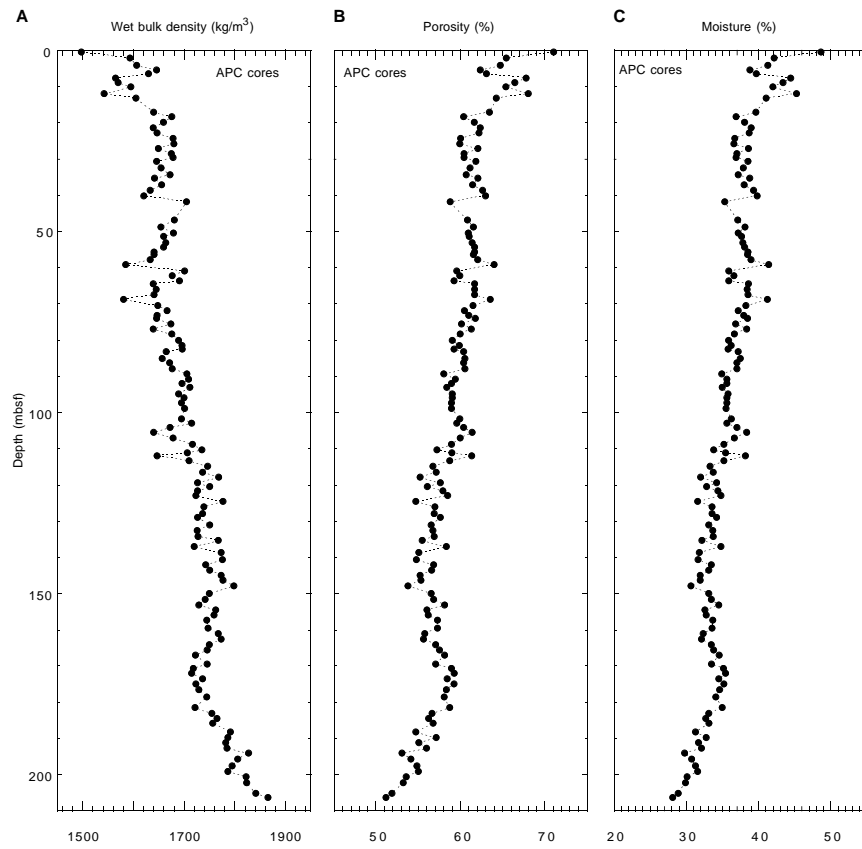


Figure 27. Index properties gravimetric (A) wet bulk density, (B) porosity, and (C) moisture content for Hole 1086A.